frontiers in Marine Science

ORIGINAL RESEARCH
published: 12 April 2019
doi: 10.3389/fmars.2019.00173

First ROV Exploration of the Perth Canyon: Canyon Setting, Faunal Observations, and Anthropogenic Impacts

Julie A. Trotter[1], Charitha Pattiaratchi[2], Paolo Montagna[3,4], Marco Taviani[3,5,6], James Falter[2], Ron Thresher[7], Andrew Hosie[8], David Haig[2], Federica Foglini[3], Quan Hua[9] and Malcolm T. McCulloch[2,10]*

[1] School of Earth Sciences and UWA Oceans Institute, The University of Western Australia, Perth, WA, Australia, [2] Oceans Graduate School and UWA Oceans Institute, The University of Western Australia, Perth, WA, Australia, [3] Istituto di Scienze Marine, Consiglio Nazionale delle Ricerche, Venice, Italy, [4] Laboratoire des Sciences du Climat et de l'Environnement, Gif-sur-Yvette, France, [5] Stazione Zoologica Anton Dohrn, Naples, Italy, [6] Biology Department, Woods Hole Oceanographic Institution, Woods Hole, MA, United States, [7] Marine and Atmospheric Research, Commonwealth Scientific and Industrial Research Organization, Hobart, TAS, Australia, [8] Western Australian Museum, Welshpool, WA, Australia, [9] Australian Nuclear Science and Technology Organisation, Kirrawee, NSW, Australia, [10] ARC Centre of Excellence for Coral Reef Studies, The University of Western Australia, Perth, WA, Australia

OPEN ACCESS

Edited by:
Cristina Gambi, Polytechnical University of Marche, Italy

Reviewed by:
Cristina Linares, University of Barcelona, Spain
Saskia Brix, Senckenberg Museum, Germany

***Correspondence:**
Julie A. Trotter
julie.trotter@uwa.edu.au

Specialty section:
This article was submitted to Deep-Sea Environments and Ecology, a section of the journal Frontiers in Marine Science

Received: *21 December 2018*
Accepted: *18 March 2019*
Published: *12 April 2019*

Citation:
Trotter JA, Pattiaratchi C, Montagna P, Taviani M, Falter J, Thresher R, Hosie A, Haig D, Foglini F, Hua Q and McCulloch MT (2019) First ROV Exploration of the Perth Canyon: Canyon Setting, Faunal Observations, and Anthropogenic Impacts. Front. Mar. Sci. 6:173. doi: 10.3389/fmars.2019.00173

This study represents the first ROV-based exploration of the Perth Canyon, a prominent submarine valley system in the southeast Indian Ocean offshore Fremantle (Perth), Western Australia. This multi-disciplinary study characterizes the canyon topography, hydrography, anthropogenic impacts, and provides a general overview of the fauna and habitats encountered during the cruise. ROV surveys and sample collections, with a specific focus on deep-sea corals, were conducted at six sites extending from the head to the mouth of the canyon. Multi-beam maps of the canyon topography show near vertical cliff walls, scarps, and broad terraces. Biostratigraphic analyses of the canyon lithologies indicate Late Paleocene to Late Oligocene depositional ages within upper bathyal depths (200–700 m). The video footage has revealed a quiescent 'fossil canyon' system with sporadic, localized concentrations of mega- and macro-benthos (~680–1,800 m), which include corals, sponges, molluscs, echinoderms, crustaceans, brachiopods, and worms, as well as plankton and nekton (fish species). Solitary (*Desmophyllum dianthus*, *Caryophyllia* sp., *Vaughanella* sp., and *Polymyces* sp.) and colonial (*Solenosmilia variabilis*) scleractinians were sporadically distributed along the walls and under overhangs within the canyon valleys and along its rim. Gorgonian, bamboo, and proteinaceous corals were present, with live *Corallium* often hosting a diverse community of organisms. Extensive coral graveyards, discovered at two disparate sites between ~690–720 m and 1,560–1,790 m, comprise colonial (*S. variabilis*) and solitary (*D. dianthus*) scleractinians that flourished during the last ice age (~18 ka to 33 ka BP). ROV sampling (674–1,815 m) spanned intermediate (Antarctic Intermediate Water) and deep waters (Upper Circumpolar Deep Water) with temperatures from ~2.5 to 6°C. Seawater CTD profiles of these waters show consistent physical and chemical conditions at equivalent depths between dive sites.

Their carbonate chemistry indicate supersaturation ($\Omega_{calcite}$ ~ 1.3–2.2) with respect to calcite, but mild saturation to undersaturation ($\Omega_{aragonite}$ ~ 0.8–1.4) of aragonite; notably some scleractinians were found living below the aragonite saturation horizon (~1,000 m). Seawater $\delta^{13}C$ and nuclear bomb produced $\Delta^{14}C$ compositions decrease in the upper canyon waters by up to ~0.8‰ (<800 m) and 95‰ (<500 m), respectively, relative to measurements taken nearby in 1978, reflecting the ingress of anthropogenic carbon into upper intermediate waters.

Keywords: Perth Canyon, deep-sea coral, oceanography, south-west Australia, remotely operated vehicle

INTRODUCTION

Submarine canyons are recognized as a key feature of continental-shelf margins and, depending on their mode of formation, geomorphology, and location on the shelf, can serve various important functions (Würtz, 2012; Huang et al., 2014; Fernandez-Arcaya et al., 2017). These canyon systems are of primary ecological importance in terms of biodiversity hotspots and ecosystem dynamics, so are increasingly the focus of interdisciplinary research (De Leo et al., 2010; McLain and Barry, 2010; de Vos et al., 2014; Huvenne and Davies, 2014; Quattrini et al., 2015; Bargain et al., 2018). Among the most prominent inhabitants of deep submarine canyons are cold-water corals, which can play important habitat-forming roles, however, the vast majority of information is limited to the Atlantic and Mediterranean regions (Morris et al., 2013; Angeletti et al., 2014; Brooke and Ross, 2014; Cordes et al., 2017; Fabri et al., 2017; Taviani et al., 2017; van den Beld et al., 2017).

As shown by visual surveys, submarine canyons are not immune to direct anthropogenic threats, such as fishery practices, dumping of waste, littering, shipping activities, and oil and gas operations (Orejas et al., 2009; Fabri et al., 2014; Daly et al., 2018; Taviani et al., 2019). Active canyon systems can be flushed by cascading shelf waters (Canals et al., 2006; Trincardi et al., 2007) that act as conduits for transporting terrestrial and coastal-sourced pollutants into deep waters, however, their impacts on deep-sea ecosystems are still to be fully assessed (Koenig et al., 2013). Such observations indicate that deep-sea canyon habitats require proper management and governance to ensure their health, integrity, and hence environmental importance (Company et al., 2012; Davies et al., 2014; Fernandez-Arcaya et al., 2017; Lo Iacono et al., 2018).

While some canyon systems represent the sub-sea extension of large river systems, transporting terrestrial sediments across the shelf to the deep-sea ocean basins, many submarine canyon systems have no direct landward connection so are largely isolated from terrestrial inputs. This latter class of canyons may be confined either to the more steeply dipping edge of the shelf-slope, or occasionally deeply incise the main shelf margin as in the case of the Perth Canyon (Harris and Whiteway, 2011; Huang et al., 2014). Previous studies of the Perth Canyon system have been confined to very limited dredge sampling and bathymetry (Marshall et al., 1989; Heap et al., 2008) or opportunistic ship-based characterization of its water masses (Woo and Pattiaratchi, 2008; Rennie S.J. et al., 2009; Rennie S. et al., 2009). Located in an oligotrophic environment with low primary production, the canyon is mainly influenced by the Leeuwin Undercurrent (LU) where subsurface upwelling occurs which is suspected to effect productivity and biodiversity in the upper reaches of the canyon (Woo and Pattiaratchi, 2008; Rennie S. et al., 2009). The canyon is known as a seasonal feeding-ground for migratory mega-fauna such as sharks and whales (Rennie S. et al., 2009), especially at the head of the canyon. However, virtually nothing was known about the deep-water invertebrate inhabitants of this canyon prior to this study.

Although relatively isolated, the unique deep-sea communities inhabiting submarine canyons are nevertheless vulnerable to anthropogenic warming and ocean acidification, which have been registered within shallow marine environments worldwide (e.g., Sabine et al., 2004; Orr et al., 2005). With rising levels of anthropogenic CO_2, the carbonate saturation horizon in the oceans is expected to rise by ~100 m to ~300 m by the year 2100 (Orr et al., 2005). This is likely to have severe consequences (Roberts et al., 2006), especially on deep-sea biota that precipitate carbonate skeletons (e.g., corals, molluscs, echinoderms) which are subject to the combined effects of reduced calcification as carbonate saturation state decreases, and increased dissolution of their skeletons as ambient canyon waters become more corrosive (Thresher et al., 2011; McCulloch et al., 2012). Being near the south-eastern Indian Ocean margin (115°E, 32°S), a largely unstudied region sourced by Southern Ocean waters, the Perth Canyon represents a prime location for studying changes in the ocean-climate system and their impacts on deep-sea ecosystems.

This first ROV-based multi-disciplinary study of the Perth Canyon investigates the main geo-biological, oceanographic, and chemical characteristics of this unique, previously unexplored, inactive canyon system. Our key goals were to: (1) strategically sample and document deep-sea corals, and (2) characterize habitat conditions and anthropogenic impacts within the canyon. Here, we characterize the canyon, its environments, and provide an overview of the faunas encountered. The environmental data is also central to constraining geochemical proxy analyses of the coral skeletons now underway, which will be used to reconstruct long-term environmental changes in the canyon. This study therefore establishes a much-needed baseline for future work focused on understanding the functioning of this canyon system, and the vulnerability of its inhabitants to the impacts of climate change and ocean acidification.

GEOLOGICAL SETTING

The canyon is surprisingly poorly understood despite being located only ∼27 nautical miles (50 km) offshore Perth, the main population center and capital city of Western Australia. Its formation is somewhat enigmatic, being subject to controversy due to the lack of connectivity to the nearby Swan River and the now passive nature of the western Australian continental margin.

The canyon resides within the Vlaming sub-basin, a pull-apart basin (Marshall et al., 1989) that formed during the separation of greater India from the western margin of the Australian continent, which concluded by the Early Cretaceous (∼134–137 Ma). Structural analysis by Marshall et al. (1989) indicates that the canyon is delineated by these pre-existing rift related fault structures, with both the NE–SW and SE–NW trending canyon tributaries apparently aligned with several transfer faults, and the head of the canyon defined by a small WNW trending graben (Marshall et al., 1989).

It has also been suggested that the canyon's incision into the continental slope is related to sub-aerial palaeo-drainage patterns carved by the adjacent Swan River when it formed part of a larger river system (von der Borch, 1968; Playford et al., 1976; Seddon, 2004). Although the canyon lies adjacent to the mouth of the Swan River, there is however no Cenozoic geomorphological evidence for any direct connectivity between the Swan River and the head of the submarine canyon. This is also the case during Quaternary periods of low sea level stands (∼120 m) where there is little evidence for the seaward migration of the Swan River mouth that could account for the extent of shelf-edge incision represented by the canyon. However, this does not preclude the possibility that a much more dynamic palaeo-Swan River drainage system provided precursor structures for the Perth Canyon, the initial uplift and down-cutting associated with either the late Jurassic-Early Cretaceous rifting of India from the western Australian margin, and/or the Late Cretaceous (mid-Santonian) breakup of Antarctic from the southern Australian margin (Exon et al., 2005).

Although the Perth Canyon is one of the few examples of significant incision into the Australian shelf-edge margin (Heap et al., 2008), its formation appears to be a result of tectonic controls along pre-existing basin structures, together with more recent (Tertiary) over steepening of shelf-edge sediments inducing submarine mass flow deposits and large-scale canyon cutting as observed in the Albany canyons (Exon et al., 2005). Given that the western Australian shelf edge is part of a passive margin, the timing of this incision event or events remain poorly constrained except that they cut the youngest sediments (i.e., Miocene).

Prior studies (Marshall et al., 1989; Shafik, 1991; Heap et al., 2008) of the canyon geology and biostratigraphy are based on dredge samples collected during the 1988 *RV Rig Seismic* expedition (BMR Cruise 80). These variably lithified limestones, shale/mudstones, and sandstones yielded foraminifer and nannofossil ages ranging mostly from Late Cretaceous to Early Miocene (Marshall et al., 1989; Shafik, 1991), and palynomorph ages between the Middle Cretaceous and Permian (Marshall et al., 1989). The depositional environments have been interpreted as varying from shallow marine to estuarine facies associated with the Swan River palaeo-drainage system (Playford et al., 1976; Quilty, 1978).

OCEANOGRAPHIC SETTING

In general, the influence of a submarine canyon on the circulation, and therefore ecology, depends mainly on the configuration of the continental shelf and slope irrespective of the forcing characteristics of the circulation. Important parameters are the continental shelf depth, canyon depth below the shelf, canyon width, canyon length, canyon's distance from the coast, the canyon's intrusion into bay areas, and the depth of the canyon mouth. The interaction between shelf and slope current systems causes localized flow patterns, which influence the ecology in the canyon's vicinity. The Perth Canyon is mainly influenced by the Leeuwin Current System (Pattiaratchi and Woo, 2009) particularly the Leeuwin Current (LC) and the LU. The LC is a surface current system (0–300 m) that transports warmer, less saline, nutrient poor waters of tropical origin southward while the LU is a subsurface (350–800 m) current that transports higher oxygen water, formed south of Australia, northward (Wijeratne et al., 2018).

The influence of the LC is limited to the upper 300 m and so does not play a major role in the dynamics of the canyon. Thus, the canyon's influence on the LC dynamics is limited to the canyon head. However, the curvature of the continental shelf in the vicinity of the canyon and the separation of the LC from the continental shelf forms anticlockwise eddies at the surface, particularly during the winter (Rennie S. et al., 2009). The main influence within the canyon is through the LU. Field measurements (Rennie S.J. et al., 2009) and numerical studies (Rennie S. et al., 2009) have indicated that circulation within the canyon is temporally variable with few repeated flow patterns. Strong vertical stratification and current shear occur at water depths of 300–350 m, at the interface between the LC and LU. The interaction between the LU and the canyon generates eddies that form over periods of 5–10 days, migrate offshore, which are replaced by newly formed eddies within the canyon. Eddies within the canyon are cyclonic and thus favor upwelling in their center. Eddies are initially confined to the canyon and then migrated offshore; however, at least one eddy, even if weak, is present in the canyon at any given time (Rennie S. et al., 2009).

The LC water consists of surface water of tropical origin (TSW, warmer, lower salinity) and South Indian Central Water (higher salinity) whist the LU transports Subantarctic Mode Water (SAMW, higher dissolved oxygen). Other water masses present within the canyon include Antarctic Intermediate water (AAIW) and Upper Circumpolar Deep Water (UCDW) (Woo and Pattiaratchi, 2008).

MATERIALS AND METHODS

The Perth Canyon cruise, FK150301, was undertaken in the early austral autumn from March 1st to 12th, 2015, aboard

the *RV Falkor*, the research vessel of the philanthropic Schmidt Ocean Institute. We used the *Falkor*'s CTD Rosette for seawater sampling, and multi-beam sonars for high-resolution bathymetric mapping. A Sub-Atlantic Comanche 2,000 m ROV, operated by Neptune Marine Services, was employed for the strategic sampling of key megabenthos from six dive sites (comprising nine dives) and to record video imagery during each dive. Continuous video footage and still photographs were taken automatically at 20 s intervals throughout each of the dives. Additional still photographs were captured manually as required. Two dive sites (A, B) are located at the head of the canyon in the east, two (C, D) are in the south near the sharp junction of the main canyon valleys, and two are in the northwest near the canyon mouth (E) and above the canyon on the upper northern plateau (F). The geology of the canyon and surrounding shelf is captured by video footage and observations recorded in the dive event logs. A suite of bathymetry maps were generated post-cruise at different spatial resolutions (see below), which depict the overall canyon system as well as localized topographic features at each of the ROV dive locations where sampling was undertaken. Additional geological information has been gathered from spot sampling of rocks and sediments from the substrate, canyon walls, and plateau. A list of all samples collected during the cruise encompassing seawater, biological, and geological samples as well as complementary datasets are reported in the SOI Cruise FK150301 Final Report[1] (McCulloch et al., 2017). The dive numbers in the figures and tables relate to the nine ROV survey and faunal collection dives only, so are offset by one from SOI D07 that was the USBL recovery dive. Specimens collected during the cruise have been deposited with the Western Australian Museum, and samples identified for geochemical analysis are held at the University of Western Australia.

Multibeam Bathymetric Analysis

High-resolution bathymetric data were acquired using Kongsberg EM 302 and 710 multi-beam echo sounders. Post-cruise, bathymetry maps of the canyon and all dive sites were generated at different spatial resolutions. The multi-beam echo-sounder data was processed using CARIS HIPS and SIPS 7.0 software. After loading raw data and applying tide corrections, the data were 'cleaned' using the Swath Editor that consists of interactively selecting and rejecting soundings as well as filtering functions, which automatically detected and rejected outliers. Following data correction and cleaning, a digital terrain model (DTM) was generated at 20 m resolution for the entire canyon (**Figure 1**), and at 10 m resolution for the ROV dive areas (**Figures 2–4**). The DTMs were exported in ASCII ESRI format and analyzed with ArcGIS 10.2. The ArcGIS Spatial Analyst tool was applied to derive the hill shade from the DTM with a vertical exaggeration of 1.5.

Seawater Collection and Analyses

Water samples (n = 59, **Supplementary Table 1**) were collected between 15 and 2,000 m from five of the dive sites (A–C, E–F) using 12L Niskin bottles mounted on a Rosette system equipped with a Seabird SBE 9plus CTD, with a SBE 43 dissolved oxygen sensor and Wet Labs ECO-FLNTU. Water column profiles are based on 59 measurements of temperature (T), salinity (S), dissolved oxygen (DO), chlorophyll *a* concentration (Σchl*a*, via water column fluorescence), total alkalinity (TA), dissolved inorganic carbon (DIC), and dissolved inorganic nutrients, together with calculations to determine the full suite of carbonate chemistry parameters. Seawater TA was measured on board by

[1]https://schmidtocean.org/cruise/perth-canyon-first-deep-exploration/

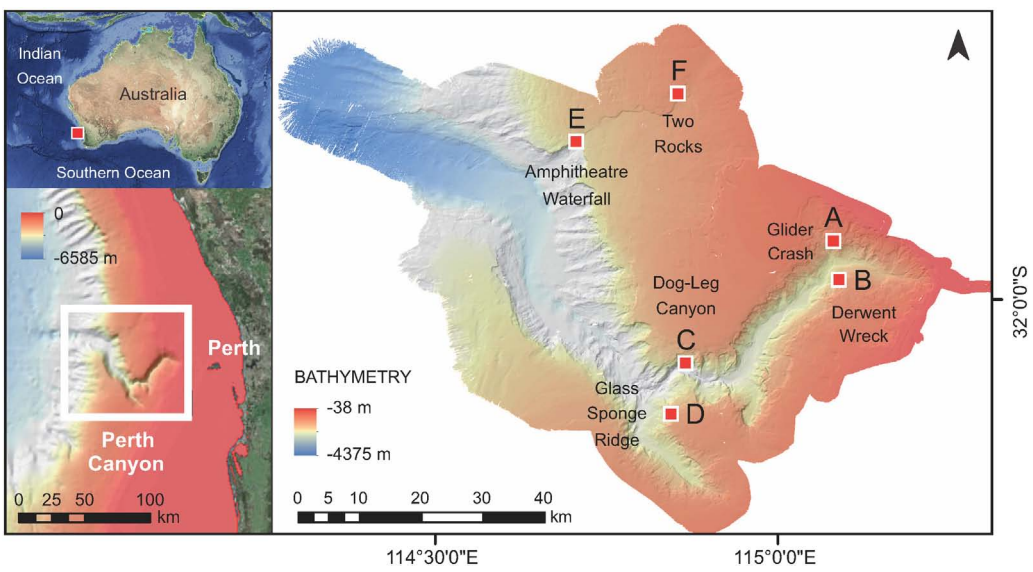

FIGURE 1 | Satellite images of the location of the Perth Canyon and bathymetry map. Bathymetry map (right) prepared from multi-beam sonar data taken during the *RV Falkor* cruise. Location of the six ROV dive surveys (Sites A–F) are indicated. Note the lack of connectivity of the canyon to the coast (bottom left).

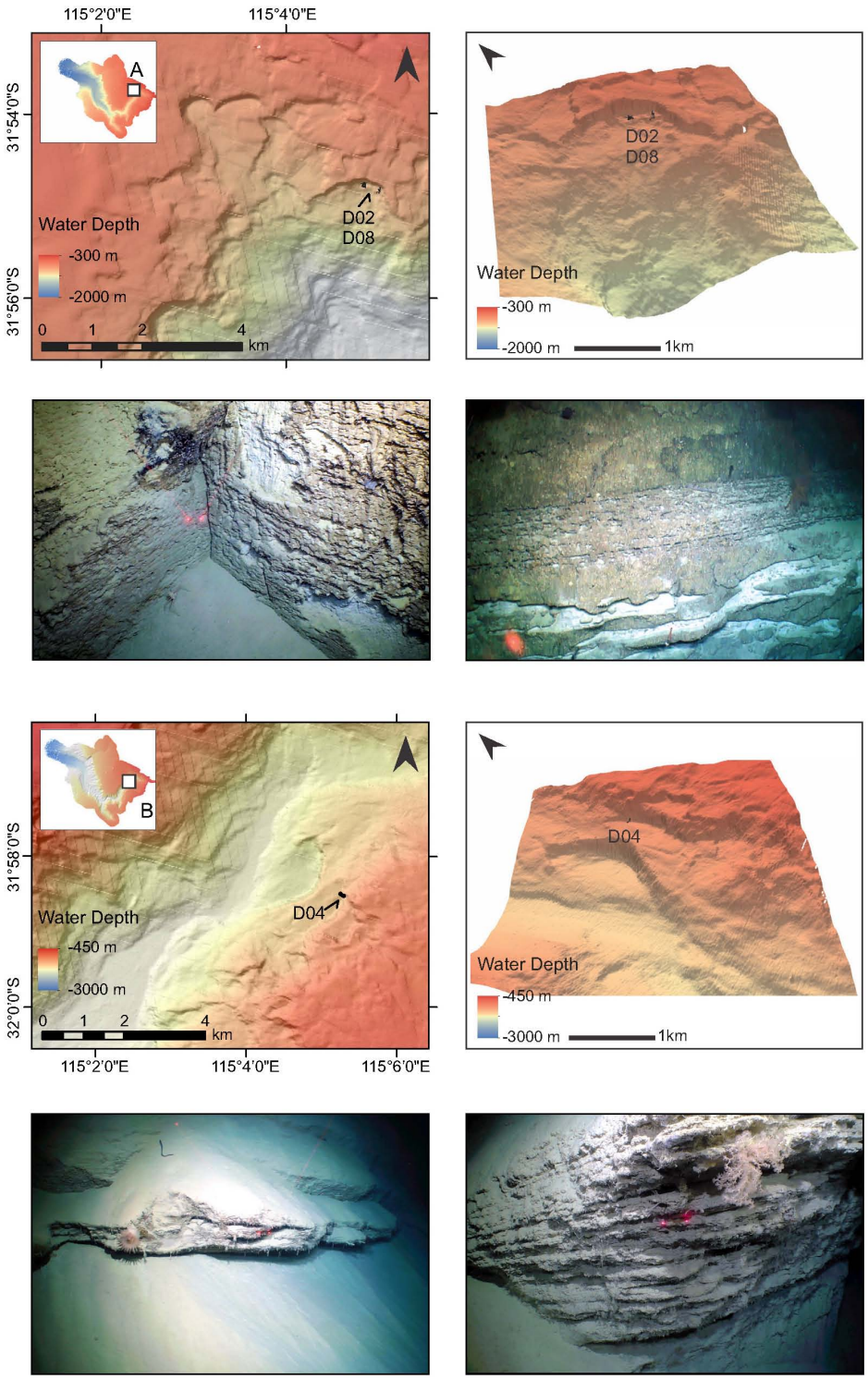

FIGURE 2 | High-resolution bathymetry maps and photos of lithologies of the canyon walls and substrates at ROV dive Sites A and B (note insets), located in the northeast region of the canyon system. Black lines on the bathymetry maps depict ROV tracks, with each dive number indicated.

single-point titration based on spectrophotometric measurement of the end-point pH (Yao and Byrne, 1998). Seawater DIC was measured on board using an Apollo SciTech Dissolved Inorganic Carbon analyzer. Dissolved inorganic nutrients, including ammonium (NH_4^+), nitrate+nitrite (commonly referred to as just 'nitrate' or NO_3^-), phosphate (HPO_4^{2-}), and silica

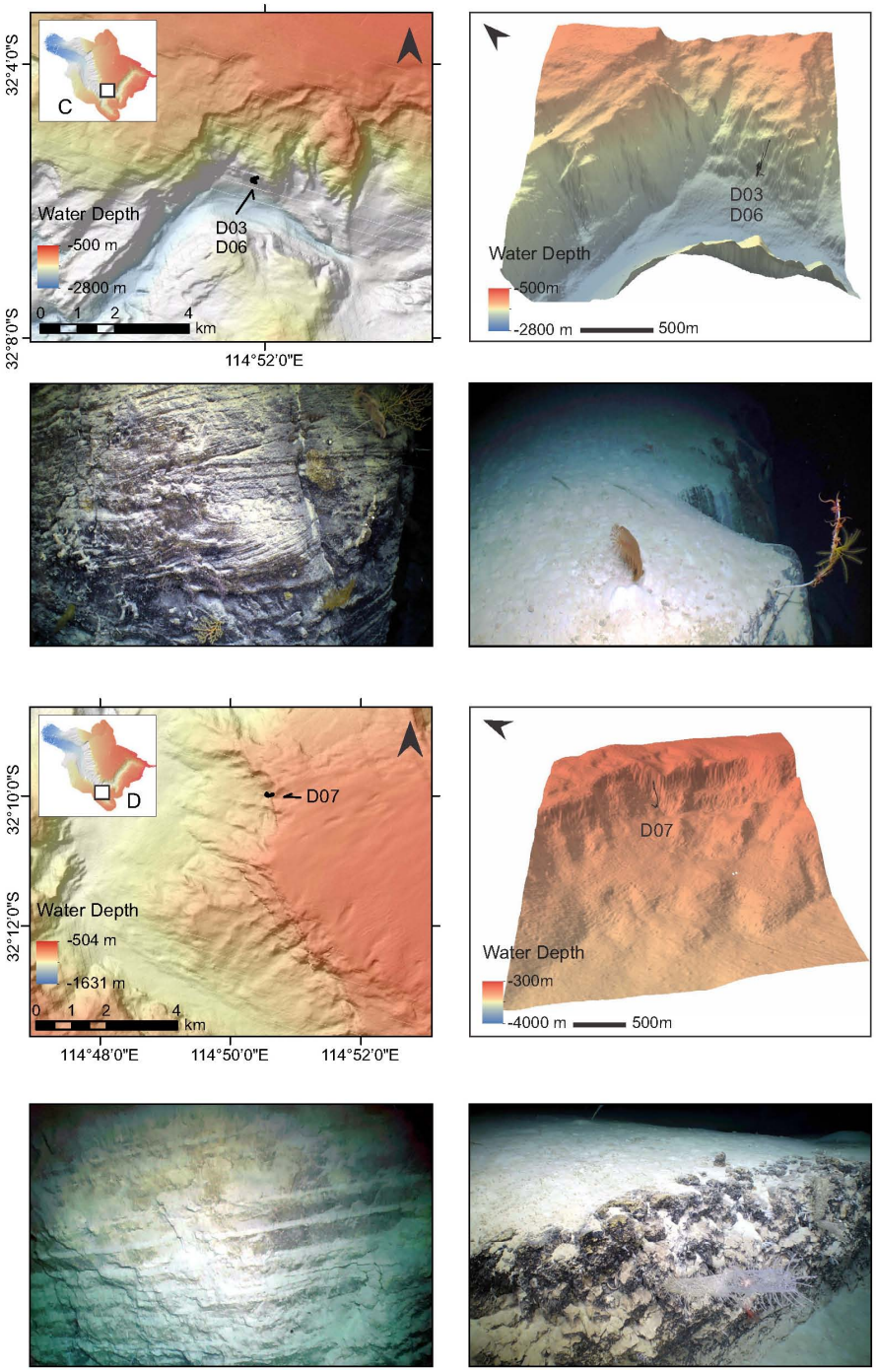

FIGURE 3 | High-resolution bathymetry maps and photos of lithologies of the canyon walls and substrates at ROV dive Sites C and D (note insets), located in the southern region of the canyon system. Black lines on the bathymetry maps depict ROV tracks, with each dive number indicated.

$[Si(OH)_4]$ were analyzed at the University of Western Australia on a Lachat autoanalyzer using standard spectrophotometric methods. Seawater pH, pCO_2, calcite saturation state ($\Omega_{calcite}$), and aragonite saturation state ($\Omega_{aragonite}$) were calculated post-cruise using MATLAB version 1.1 of the CO2SYS software (van Heuven et al., 2011).

Stable C and O isotope measurements of 29 seawater samples from five sites (A: n = 9, B: n = 9, E: n = 11) were undertaken in the West Australian Biogeochemistry Centre at The University of Western Australia. The stable isotope compositions of oxygen and hydrogen were analyzed using an Isotopic Liquid Water Analyzer Picarro L1115-i. Each sample was analyzed six times

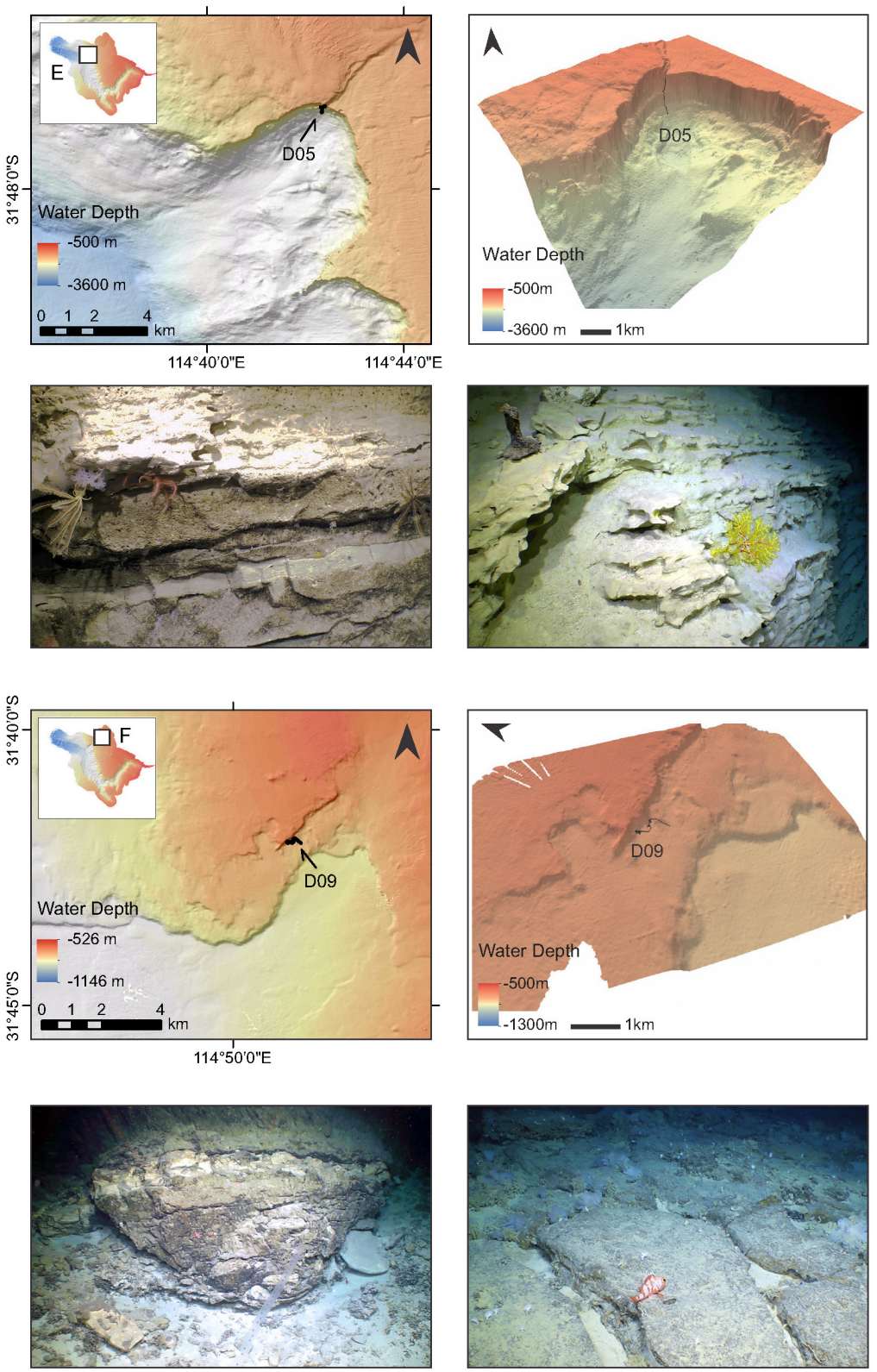

FIGURE 4 | High-resolution bathymetry maps and photos of lithologies of the canyon walls and substrates at ROV dive Sites E and F (note insets), located in the western region of the canyon system. Black lines on the bathymetry maps depict ROV tracks, with each dive number indicated.

and then the first four results were discarded in order to minimize any instrument memory effect. The δ^2H and $\delta^{18}O$ raw values of samples were normalized to the Vienna Standard Mean Ocean Water (VSMOW) scale, based on three laboratory standards, each replicated twice and reported in per mil (‰) following the principles of the three-point normalization (Skrzypek, 2013). All laboratory standards were calibrated against international reference materials that determine the VSMOW-SLAP scale (Coplen, 1996), provided by the International Atomic Energy Agency (for VSMOW2 δ^2H and $\delta^{18}O$ of equal 0‰ and for SLAP equal $\delta^2H = -428.0$‰ and $\delta^{18}O = -55.50$‰). The long-term analytical uncertainty (1σ) was determined as <1.0‰ for δ^2H and <0.1‰ for $\delta^{18}O$ (Skrzypek and Ford, 2014). The stable carbon isotope composition of DIC was analyzed using a Thermo-Fisher GasBench II coupled with Delta XL Isotope Ratio Mass Spectrometer. Prior water sample injection, 12 mL vials with 0.1 mL of 100% phosphoric acid were flushed with ultra-high purity helium (99.999%), and then reacted at 25°C for 24 h (Paul and Skrzypek, 2006). The water volumes of samples were adjusted accordingly in order to match the peak heights of reference materials and avoid the linearity effect. All results were expressed using the standard delta-notation ($\delta^{13}C$) and were reported in per mil (‰) after normalization to Vienna Pee Dee Belemnite isotope scale (VPDB). The multi-point normalization was based on three international standards NBS18, NBS19, and L-SVEC for $\delta^{13}C$, each replicated twice (Skrzypek, 2013). The analytical uncertainty was $\leq \pm 0.1$‰ (1σ).

Radiocarbon (^{14}C) analyses of 20 seawater samples collected from five sites (A–C and E, F) were undertaken at the Australian Nuclear Science and Technology Organisation (ANSTO). DIC of seawater (40–60 mL) was stripped out as CO_2 by acidifying the samples with 85% H_3PO_4 (5 mL), which was carried out in a custom-built extraction line by sparging the acidified water with He gas for 15 min. The gas was recirculated, passing through two dry ice/ethanol traps to remove water, and a LN_2 trap to condense the sample CO_2. Following removal of the He and other incondensable gasses, the CO_2 was converted to graphite using the H_2/Fe method (Hua et al., 2001). A portion of graphite was used for the determination of $\delta^{13}C$ for isotopic fractionation correction using a Micromass IsoPrime elemental analyzer/isotope ratio mass spectrometer (EA/IRMS). Accelerator mass spectrometry (AMS) ^{14}C analysis was conducted using the STAR facility at ANSTO (Fink et al., 2004), with a typical analytical precision of better than 0.35% (1σ). Oxalic acid I (HOx-I) was used as the primary standard for AMS ^{14}C determination, and oxalic acid II (HOx-II) and IAEA-C7 reference material were employed as secondary standards. The AMS results are presented in $\Delta^{14}C$, the per mil deviation from the absolute radiocarbon standard (Stuiver and Polach, 1977).

CTD-Rosette data were visualized using the Ocean Data View software (version 4.7.10), and all graphs of seawater parameters discussed above have been generated using this program.

Faunal Sampling and Descriptions

The ROV was used to collect megabenthos during each dive. Sampling mainly targeted deep-sea corals, especially those that precipitate carbonate skeletons given their suitability for geochemical proxy studies, which are ongoing. Faunal descriptions (see section "Canyon Fauna") are mostly based on real-time observations of video footage that were recorded in event logs during the cruise, with subsequent identifications undertaken post-cruise on hand samples collected by the ROV. Taxonomic identifications are either to genus or species level where possible, however, specialist taxonomic research with publications are expected to be produced in the future. Faunal lists of samples collected by ROV can be found in the SOI Cruise FK150301 Final Report (McCulloch et al., 2017; see footnote 1), and vouchers of collected specimens have been deposited with the Western Australian Museum, Perth.

U-Th Dating of Corals

Absolute ages were determined by the uranium-thorium (^{238}U–^{230}Th) series decay technique for 28 fossil coral specimens (n = 31) collected at two ROV dive sites spanning a depth range of 691–1,788 m. Subsamples were extracted from the fossil skeletons of *Desmophyllum dianthus* (Esper, 1794) and *Solenosmilia variabilis* (Duncan, 1873), using a dental drill with diamond-encrusted blades and burs. The subsamples were first mechanically cleaned with the drill then crushed in an agate mortar and pestle. Aliquots of ∼20 to ∼50 mg were lightly leached in 0.1N HCl, dissolved in dilute HCl and spiked with enriched ^{229}Th, ^{233}U, and ^{236}U tracers. Uranium and thorium were extracted from 3N HNO_3 sample solutions using Eichrom UTEVA ion exchange chromatography resin following the procedure of Douville et al. (2010). All U-Th measurements were carried out on a Thermo Scientific Neptune Plus MC-ICPMS equipped with a jet interface and a desolvation system yielding an overall ion efficiency of 2–3%. The ^{238}U signal was collected using a 10^{10} Ω amplifier, allowing signal intensities for ^{238}U of >100 V. U samples and bracketing standard CRM 112-A were spiked with reference material IRMM-3636a to correct for mass bias and yield drift of the SEM. Additional corrections were applied for tailing and hydride generation. For Th determinations, ^{229}Th-spiked samples were bracketed against IRMM-3636a, with specific attention given to maximize washout of ^{230}Th between samples. Using U as the bracketing standard for Th may introduce some uncertainty from differential mass bias behavior, however, no suitable Th standard was available and errors from mass bias correction are generally smaller (<1‰) than errors from counting statistics on ^{230}Th alone (∼3–8‰). Activity ratios for $^{230}Th/^{238}U$ and $^{234}U/^{238}U$ were then calculated using the decay constants and reference values given in Jaffey et al. (1971) and Cheng et al. (2013), but calibrating the $[^{230}Th/^{238}U] = 1$ for Harwell Uraninite HU-1 assuming secular equilibrium, and using $\delta^{234}U = -38.5$‰ for CRM112-A. Analytical uncertainty for $\delta^{234}U$ derived from repeated determinations of HU-1 was 0.8‰ (2σ; n = 30), whereas errors on $[^{230}Th/^{238}U]$ strongly depend on ^{230}Th counting statistics and minor blank/washout corrections, and ranged from ∼2.8‰ (2σ; n = 30) for HU-1 to 8.3‰ (2σ; n = 12) for very young samples (e.g., CRM112-A). Total procedural blanks were typically on the order of ∼30 attograms for ^{230}Th and ∼12 femtograms for ^{238}U, which are considered negligible. Ages

were calculated through iterative age estimation (Ludwig and Titterington, 1994) and assuming the initial non-radiogenic [^{230}Th/^{232}Th] = 2 (±1) then calibrated to the year 1950 (i.e., BP). All samples were prepared and analyzed in the Advanced Geochemical Facility for Indian Ocean Research at the University of Western Australia.

Geological Samples

Several geological 'spot' samples were collected using the ROV robotic arm. Foraminiferal biostratigraphy, palaeo-bathymetry, and lithologies have been determined from a selection of nine geological samples from four dive sites (A, D–F). Seven friable to partly friable samples were disaggregated in water and the washed sand fractions examined under a stereomicroscope. Samples of wackestone and chert were examined in thin section. The samples investigated were from depths of 1,603 m (FPC-15 D05-S01), 1,241 m (FPC-D05-S08), 1,032 m (FPC-D07-S05), 746–716 m (FPC-15 D09-S01, S02, S04) and 701 m (D08-S03). The biostratigraphy of these samples was determined from planktonic foraminiferal associations and the palaeo-bathymetry from benthic foraminiferal assemblages.

The strontium (Sr) isotopic compositions (^{87}Sr/^{86}Sr) were also undertaken to date some lithologies from the canyon wall. Sediments were sampled from the basal holdfasts of eight deep-water corals together with seven rock samples from five dive sites (A, B, D–F). Sediments extracted from coral holdfasts were from depths of 1,472 m (Site E D05-S03, live *Vaughanella*), 936 m (Site B D04-S01, live and fossil *Desmophyllum* and fossil *Solenosmilia* sampled from the same colony), 739 m (Site F D09-S02, live *Polymyces*), 701 m (Site A D08-S03, recently dead *Polymyces*), and 675 m (Site A D08-S05, live *Caryophyllia*). Sample collection D09-S2 was from a small boulder sitting on the substrate. Rock analyses were of subsamples from well-consolidated mudstone units sampled from the canyon wall at 1,444 m (Site E D05-S04 mudstone) and 1,032 m (Site D D07-S05), as well as soft, friable mudstone nodules collected from the shallower depths at 746 m (Site F D09-S01), 716 m (Site F D09-S04), and 701.3 m (Site A D08-S3). Collection D09-S02 comprises loose debris that was scooped from the substrate. The very small size and preservation of the foraminifers made them unsuitable for isotope analysis, thus precluding comparative Sr analysis of the host rocks and microfossils that were used for biostratigraphy.

Strontium was separated from 10 mg carbonate aliquots by ion exchange chromatography using Eichrom Sr Resin. All Sr isotopic compositions were measured in solution using the Thermo Scientific Neptune Plus housed in the Advanced Geochemical Facility of Indian Ocean Research at the University of Western Australia. Averages of standard ^{87}Sr/^{86}Sr measurements from two analytical sessions gave NBS SRM987 = 0.710299 (n = 7) and 0.710283 (n = 4), with analytical uncertainties at 95% confidence limits of 0.000015 and 0.000004, respectively. The instrumental mass fractionation was corrected using a stable isotopic ratio of ^{86}Sr/^{88}Sr of 0.1194 and an exponential law. ^{87}Sr/^{86}Sr measurements of the sample unknowns were normalized to 0.710248 to determine their Sr ages using the SIS Look-up Table v4:08/03 (McArthur et al., 2001).

Supplementary Oceanographic Data

The Perth Canyon region includes a range of oceanographic infrastructure that has been established as part of the Australian Integrated Marine Observing System (IMOS) and an overview of the different data streams is provided in Mihanović et al. (2016). These include oceanographic moorings that contain Acoustic Doppler Current Profilers (ADCP), surface currents measured by HF Radar, sea surface temperature from satellites and ocean glider transects. Data streams collected during the period of the *RV Falkor* voyage were abstracted from the IMOS data portal[2].

Hourly data collected by the HF Radar systems were averaged over 24 h for March 9, 2015, and was overlain over the satellite derived sea surface temperature image for that date. Velocity profiles over the period March 1–15, 2015, from within the canyon were available from an IMOS mooring located in ∼500 m water depth (31.7867°S 114.9400°E). The Teledyne RDI Workhorse Long Ranger 75 kHz instrument was mounted on the sea bed and collected data at 15-min intervals in 16 m bins through the water column from 48 to 480 m from the seabed.

Ocean gliders are autonomous vehicles that utilize a buoyancy engine to move through the water column in a saw-tooth pattern (Pattiaratchi et al., 2017). During the *RV Falkor* voyage a *Seaglider*, developed by the University of Washington was deployed in the Perth Canyon and undertook east–west transects to a maximum depth of 1,000 m. The sensors on the *Seaglider* included those for temperature, salinity, and DO (Seabird Electronics SBE41 CTD and SBE 43 DO sensor) and optical sensors for Chlorophyll fluorescence (BBFL2SLO 3 parameter optical sensor). IMOS data streams are provided in NetCDF-4 format with ocean glider data files containing meta-data and scientific data for each glider mission. Subsequent to the ocean glider recovery, all data collected by the glider are subject to QA/QC procedures that include a series of automated and manual tests (Woo, 2018).

RESULTS

Canyon Morphology and Geology

The Perth Canyon is described as long, deep, narrow, steep-sided and intruding into the continental shelf. It is characterized by two main tributaries forming a sinuous or V-shaped configuration, which initially trends SW from the canyon head, then sharply diverges to the NW toward the mouth of the canyon (**Figure 1**). The 50 m depth contour marks the uppermost incision into the continental shelf, which expands to ∼10 km wide around the canyon head, meanders for ∼120 km to the west, and reaches depths of >4,000 m. At the canyon head, the depth plunges from 170 to 1,000 m. A series of approximately right-angle bends mark the major changes in the canyon's orientation at distances of ∼10 km, 40 km, 50 km, and ∼100 km from the tip (the head's closest point to the coast). From the easternmost tip, the canyon's orientation at 0–10 km trends in a ∼SE–WNW direction, at 10–40 km it runs NE–SW, at 40–50 km it trends roughly E–W, at 50–100 km it changes to a ∼SE–NW direction, and at

[2]https://portal.aodn.org.au/

∼100–120 km the mouth follows a near westerly direction as it opens onto the abyssal ocean plain. A morphologically more complex zone occurs in the region ∼40–50 km from the tip, where the canyon's floor narrows in parts to <1 km in width and its orientation changes abruptly thus defining the major canyon bend (Site C). This main juncture at ∼50 km is joined by a short southern arm, a ∼15 km long trench of a similar morphology to the main (inshore) canyon head. The width of the canyon varies from roughly 2–5 km wide near the head, broadening to ∼10 km in the 10–40 km region, narrowing again to ∼5–8 km at Site C, and eventually expanding to ∼20 km at the mouth as it forms a large submarine fan. The walls of the canyon typically have ∼30° to 40° gradients although some parts are near vertical (Sites C and E). Broad terraces occur at the shallower sites near the canyon head (Sites A and B), and a distinctive NE trending scarp transects the northern canyon sites (E and F). Toward the mouth of the canyon, a steep walled, large arcuate terrace is reminiscent of a terrestrial amphitheater and waterfall (Site E).

Muddy substrates feature at the base of all six dive transects. Near the head of the canyon (Sites A and B) muds transition sharply to a coarse bedded vertical cliff-face with fissures and prismatic jointing. Lithologies comprised intervals of brecciated rock, interbeds of light-colored blocks with deformation indicative of slumping, mudstones and roughly eroded (karstified) chalky, friable layers of varying thickness, and thin nodular lenses. Similar lithologies are observed in the northernmost, shallow site on the canyon plateau (F), which also featured small fallen blocks, pebbles, and extensive fossil coral rubble deposits. The deepest sites (C and E) are characterized by steep canyon walls, sometimes near vertical, ∼500–600 m high, with massive blocky and jointed strata, and well-bedded consolidated units. Large muddy aprons containing masses of fossil coral deposits occur between the cliff walls (Site C). Layered mudstones, chert, large collapsed blocks, and steep walls transition to soft clay beds at the top of Site D. Other sedimentary features, such as cross-bedding (Site C), slump structures and wavy laminations (Site E), were also observed. **Figures 2–4** show bathymetry maps for each dive site together with some lithologies observed during the surveys. Additional images of canyon lithologies observed during the dives are shown in **Supplementary Figures 1**, **2**, and the ROV video footage available on the SOI website[3].

Stratigraphy and Paleobathymetry

The nine geological samples examined represent a roughly 900 m sedimentary section that comprises three distinct facies of Late Paleocene, Middle-Late Eocene, and Early Oligocene in age (**Supplementary Table 2**) that were determined by planktonic foraminiferal biostratigraphy. Strontium (Sr) isotope analyses of rocks and/or sediments from remnant host rock attached to coral holdfasts are broadly consistent with biostratigraphic ages, except those of the youngest and shallowest samples (**Supplementary Figure 3** and **Supplementary Table 2**). The paleobathymetry determined from benthic foraminifers from the *RV Falkor* samples indicate consistent upper bathyal to upper middle bathyal (200–700 m) depths throughout these Late Paleocene to Early Oligocene deposits. The Oligocene samples were probably deposited at a depth similar to the present-day water depth at Sites A and F, which are the shallowest dive sites. There is no evidence of down-slope movement of sediment from a neritic shelf environment so we assume the assemblages are *in situ*.

The co-occurrence of *Globanomalina pseudomenardii* and *Acarinina soldadoensis* in a wackestone collected at 1,602 m (Site E) indicates a Late Paleocene (Zone P4c) age of ∼56–56.5 Ma (Olsson et al., 1999). At 1,241 m (Site E), a wackestone containing *Globigerinatheka index* together with probable *G. subconglobata* and rare *Acarinina* sp., suggest a probable Middle Eocene age (zones E10–E12) of ∼40–44 Ma (Pearson et al., 2006). The presence of *Globigerinatheka* in an indurated wackestone collected at 1,032 m (Site D) indicates a Middle or Late Eocene (zones E8–E16) age of ∼34–48 Ma. The absence of distinct *Acarinina* or *Morozovelloides* may indicate an age no older than zone E12, late Middle Eocene (no older than ∼40 Ma). Wackestones collected from depths of 746 to 701 m (Sites A and F) contain foraminifera of the same age. The presence of *Catapsydrax dissimilis*, *C. unicavus*, *Ciperoella anguliofficinalis*, *Globoturborotalita ouachitaensis*, and *Dentoglobigerina tripartita* and the absence of *Globigerinatheka*, *Hantkenina*, and *Turborotalia cerroazulensis*, which are characteristic of the Late Eocene, as well as *Globigerinoides* that is characteristic of the Miocene, suggest that these samples are likely Oligocene in age. The lack of abundant *Ciperoella*, including the *C. ciperoensis* (Bolli) group of species, as well as *Dentoglobigerina binaiensis* (Koch) indicate an early Oligocene (zone O1–2) age of ∼30–33 Ma (Wade et al., 2018). For further details of the biostratigraphic analyses and paleobathymetry, see **Supplementary Data**.

The $^{87}Sr/^{86}Sr$ compositions of samples from 1,472 and 1,444 m (Site E) gave the lowest $^{87}Sr/^{86}Sr$ ratios (0.707775–0.707774), which equate to a broad range of Eocene ages (55.6–35.0 Ma) due to the non-linearity of the Sr isotope seawater curve for this period. These Sr ages are consistent with the Late Paleocene and Late Eocene biostratigraphic ages below and above these depths. The sample from 1,032 m (Site D) also yielded low $^{87}Sr/^{86}Sr$ ratios (0.707781 and 0.707794), and hence multiple possible Sr ages (45.1–35.3 Ma) between the Middle to Late Eocene, however, the inferred Middle Eocene biostratigraphic age constrains the Sr age between 43.9 and 45.1 Ma. Sediments from coral holdfasts as well as loose soft, friable, mudstone and siltstone nodules from shallower depths (936–675 m) at Sites A, B, and F, gave latest Oligocene to Early Miocene ages; for this time interval the Sr seawater curve is unidirectional and steep thus yielding single ages. Various samples from 936 m (Site B) gave consistent Early Miocene Sr ages (20.3, 20.1, and 19.8 Ma); there are no biostratigraphic ages for samples from this site for comparison. Early Miocene ages (22.0 to 17.0 Ma) were also determined from different samples types, collected between 746 and 716 m (Site F). Similarly young Sr ages, of Late Oligocene (23.9 Ma) and Early Miocene (22.4 17.6 Ma)

[3]https://schmidtocean.org/cruise/perth-canyon-first-deep-exploration/#data

were determined from various samples from depths of 701 to 675 m (Site A).

Chemical and Physical Oceanography

Structure and Chemical Compositions of Canyon Waters

The waters in and around the Perth Canyon (Sites A–C, E, F) are very similar in their physical structure and compositions (**Supplementary Figures 4–7**) and are consistent with previous studies (e.g., Woo and Pattiaratchi, 2008). Temperatures in the canyon range from ∼24°C to ∼2°C in the deepest water sampled (2,000 m). The salinities ranged between 34.4 and 35.6. The DO content ranged between ∼250 μmol kg^{-1} (300–550 m) and ∼150 μmol kg^{-1} (below 1,000 m). The major water masses in the canyon were identified based on their temperature (T), salinity (S), and DO content (**Figure 5** and **Supplementary Figure 4**) and are summarized below:

1. Tropical Surface Waters (TSW: 0–100 m) found in the surface layer associated with the LC with $T > 23.5$°C and S ∼35.5.
2. South Indian Central Water (SICW: ∼100–300 m), an intermediate upper ocean water mass also associated with the LC with $T = 16$°–22°C and with a subsurface salinity maximum at $S \geq 35.7$.
3. Subantarctic Mode Water (SAMW: >300 to ∼750 m) characterized by maxima in DO (>250 μmol kg^{-1}) and associated with the LU with $T = 8$°–15°C and a salinity decrease from 35.4 to 34.6.
4. Antarctic Intermediate Water (AAIW: ∼750 to ∼1,000 m) with $T = 4.5$°–7°C and with a salinity maximum at 34.4.
5. Upper Circumpolar Deep Water (UCDW, ∼1,000 to ∼2,000 m) with $T < 4.5$° and salinity increasing from 34.5 with lower oxygen (∼150 μmol kg^{-1}).

The $\delta^{18}O$ profile (**Supplementary Figure 5A**) shows a similar depth dependent trend to that of DO with a peak in $\delta^{18}O$. This is confirmed by the good correlation between salinity and $\delta^{18}O$ (**Supplementary Figure 5C**). The hydrogen isotope profile (**Supplementary Figure 5B**) also shows a similar pattern as the $\delta^{18}O$, consistent with the higher salinity of the upper ∼200–300 m water masses having elevated $\delta^{2}H$.

Profiles of total chlorophyll exhibit a somewhat 'noisy' but persistent sub-surface maximum of 0.25–1.0 mg m^{-3} that occurs between ∼60 and 90 m at all locations, except the northernmost site (Site F) where the maximum of 0.36 mg m^{-3} is much deeper at ∼150 m (**Supplementary Figure 6A**). The water column nutrients throughout the Perth Canyon are generated almost entirely *in situ*, as indicated by the ratio of total dissolved inorganic nitrogen (nitrate plus ammonium) to total dissolved inorganic phosphorus (SRP) being close to the idealized Redfield-Richards ratio (17.4 ± 0.4 vs. 16). The nitrate plus nitrite and soluble reactive phosphorus increase monotonically with depth (**Supplementary Figures 6B,C**). TA and DIC are similar across the canyon sites (**Supplementary Figures 7A,B**). TA has a somewhat similar profile as salinity whereas DIC increases more monotonically with depth. There is a concomitant decrease in pH and increase in pCO_2 with depth (**Supplementary Figures 7C,D**), and substantial monotonic declines of ∼75% in both calcite and aragonite saturation with depth relative to surface values (**Supplementary Figures 7E,F**). Although all waters within the Perth Canyon and surrounds

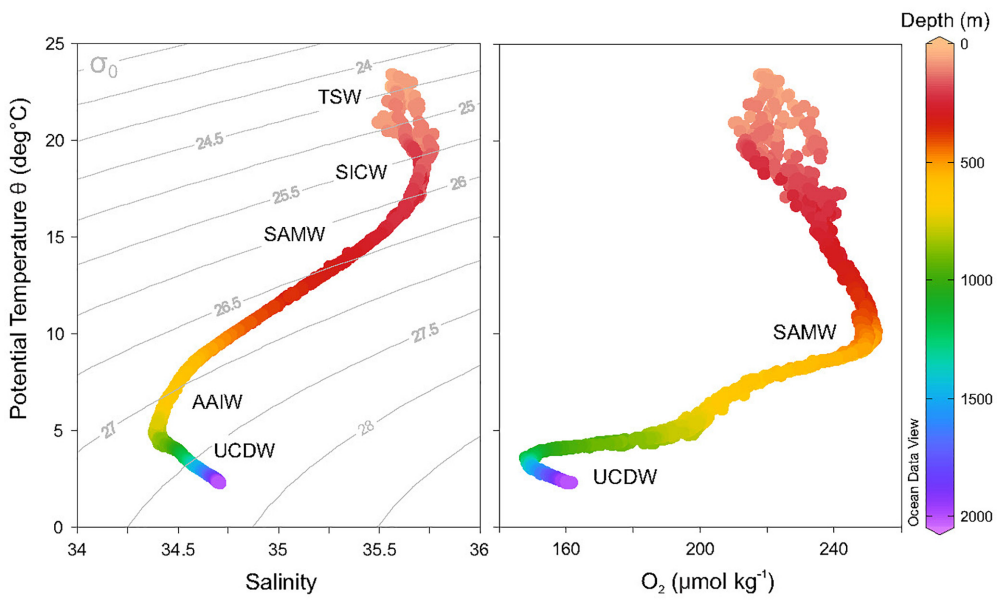

FIGURE 5 | Temperature–salinity (left) and temperature–oxygen (right) plots for Potential Temperature Depth of Perth Canyon waters with water masses indicated. TSW, Tropical Surface Water; SICW, Subtropical Indian Central Water; SAMW, Subantarctic Mode Water; AAIW, Antarctic Intermediate Water; UCDW, Upper Circumpolar Deep Water. Isopycnals calculated with the reference pressure at 0 m.

remain oversaturated with respect to calcite, waters deeper than ∼1,000 m are undersaturated with respect to aragonite thus defining the aragonite saturation horizon at this depth.

The carbon isotope ($\delta^{13}C$) compositions of the canyon waters are consistent at the three sites measured near the head and mouth of the canyon (Site A, B, E). The $\delta^{13}C$ composition initially decreases in depth within the uppermost ∼200 m (∼0.8–0.6‰), then rapidly increases to a maximum at ∼420 m (∼1.2‰), before decreasing to ∼0.4 from ∼1,200 m (**Supplementary Figure 8A**). Seawater radiocarbon ($\Delta^{14}C$) compositions also show consistent profiles (Sites B and E), ranging from 42.9 to −191.2 from surface to deep waters, showing similar compositions within the upper ∼500 m (**Supplementary Figure 8B** and **Supplementary Table 3**). These profiles are compared with $\delta^{13}C$ and $\Delta^{14}C$ profiles determined from earlier cruises undertaken in the region (**Figure 6**) to assess the uptake of anthropogenic carbon uptake over time (see section "Anthropogenic Impacts").

Canyon Hydrography

During the period of the *RV Falkor* cruise, surface currents reflected the typical summer circulation pattern in the study region. Here, the warm LC flows southward across the Perth Canyon (**Supplementary Figure 9**). On the continental shelf, the colder northward flowing Capes Current (CC) is present, driven by southerly winds. An anti-clockwise eddy forms at the surface centered at the head of the canyon (115.0°E) due to the current shear generated by the opposing currents (LC and CC) and the shoreline orientation. The warmer LC becomes spread laterally across the canyon: i.e., to the north and south of the canyon the LC is narrow but over the canyon it is much broader (**Supplementary Figure 9**).

The vertical current profiles obtained during the study period indicated evidence of strong diurnal–inertial resonance from March 1 to March 10, 2015 (**Figure 7**). Here, currents, in both the north–south and east–west components in the upper 200 m show strong oscillations that alternate between positive and negative values over each 24-h period. The winds changed after March 10, with no sea breeze events leading to cessation of the diurnal–inertial resonance and the generation of near-inertial waves. In the depth range of 200–450 m, the north–south component of the currents indicated persistent northward flow with mean currents ∼0.2 m s^{-1}, which represents the LU. The time series indicate strong current shear between the upper layer (0–200 m) that include the diurnal oscillations, and the southward LC and the northward flowing LU below (**Figure 7**).

The water properties observed with the *Seaglider* provided additional information to that obtained from the CTD casts. The temperature and salinity contours show downward tilting toward the coast (a vertical change of ∼100 m from east to west across the transect; **Figure 8**) due to the downwelling nature of the LC. The warmer (>23°C), lower salinity (<35.6) water forms only a shallow surface layer (<50 m) at the surface and a strong thermocline is present between 50 and 100 m (**Figure 8A**). The subsurface salinity maximum (>35.6) is present although at the western end of the transect it is at the surface (**Figure 8B**). The DO maximum layer present between 200 and 550 m (**Figure 8C**) indicates the SAMW associated with the LU. The other two deeper water masses present in the canyon, AAIW (750–1,000 m) and UCDW (1,000–2,000 m), were captured in the CTD casts (see section "Structure and Chemical Compositions of Canyon Waters") and the ocean glider. Chlorophyll fluorescence indicated a persistent subsurface chlorophyll maximum centered at 80 m water depth (**Figure 8D**) across the canyon and was associated with the thermocline.

Canyon Fauna

One of the shallowest ROV surveys was conducted near the head of the canyon (Site A: 663–743 m) within AAIW. Here, crabs (e.g., *Chaceon albus,* Davie, Ng and Dawson, 2007) were the common mobile megabenthos. Demersal species were represented by grenadiers and deep-sea dories, and pelagic sea-cucumbers. The canyon walls harbored polychaete tube worms, glass sponges including a new species *Amphidiscella* sp. nov., occasional echinoderms (sea urchins, crinoids, and sea stars), lobsters (**Figure 9A**) (*Projasus parkeri,* Stebbing, 1902), and the zoanthid bearing hermit crab *Sympagurus* sp. (**Figure 9B**). The first cnidarians were seen at 716 m (sea anemone and cup corals), with species richness greater near the top of the cliff where antipatharians (e.g., **Figures 9C,D**) and solitary live and sub-fossil scleractinians (*D. dianthus*, *Caryophyllia* sp., and *Polymyces* sp.) were common. A selection of cup corals, *D. dianthus*, *Caryophyllia* sp., and *Polymyces* sp. (e.g., **Figures 9E,F**), were collected between 716 m and 674 m. Two *Acesta* sp. nov. bivalves (**Figure 9G**) and a hexactinellid sponge were collected from the canyon wall nearby between 675 and 695 m, also from rough karstified beds (e.g., **Figure 9G** and **Supplementary Figure 1C**), albeit more weakly lithified that sometimes fragmented during sampling. The gorgonian *Narella* sp. (**Supplementary Figure 1E**), was collected at 695 m from the canyon wall (that also accommodated serpulid tube worms) that was well-lithified and incorporated distinctive large white clasts and lenses (e.g., **Figure 9C** and **Supplementary Figures 1E,F**); a similar substrate was also present at the northernmost shallow Site F. A non-branching bamboo coral (*Lepidisis* sp.) was collected at 679 m and one large black coral (antipatharian) was sampled at 678 m (**Figure 9D**) where the canyon wall was composed of a massive, well-lithified, and relatively featureless matrix. Soft corals were uncommon and colonial scleractinians were not observed.

During the slightly deeper dive at Site B (directly opposite Site A), we observed live and dead scleractinian corals, serpulid tube worms, brachiopods, verrucid barnacles, crustaceans (crabs and squat lobster), and the first sighting of the large glass sponges (*Walteria* sp., also at Site D) near the edge of the ridge. A sea anemone (1,079 m) and a gorgonian (probably *Narella* sp. at 1,010 m) were the deepest cnidarians observed. Coral diversity and abundance appeared markedly higher between ∼950 and 930 m. Within this range, several live but ∼20 dead (i.e., ferromanganese coated) *D. dianthus* were observed, and a dead colony of *S. variabilis* was collected at 936 m at the top of a ledge composed of coarse friable rock. This dead *S. variabilis* colony contained a single live polyp, as well as live and sub-fossil *D. dianthus* and numerous newly settled polyps (seemingly *D. dianthus*), the latter as small round dots on dead coral skeletons. Between 930 and 950 m were a moderately large

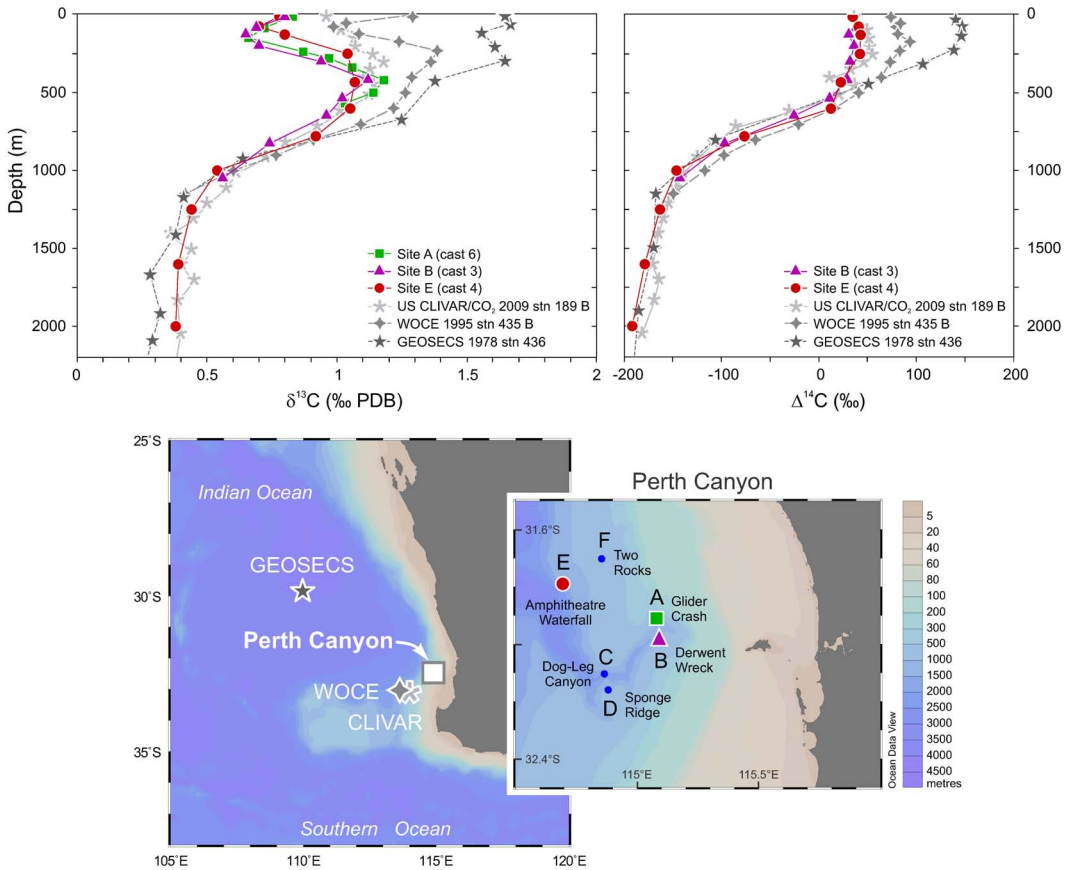

FIGURE 6 | Representative vertical profiles of seawater $\delta^{13}C$ (top left) and $\Delta^{14}C$ (top right) compositions from the Perth Canyon compared with data from earlier cruises in the region: GEOSECS (1978, station 436), WOCE (1995, station 435), and US CLIVAR/CO2 (2009, station 189). Satellite map (bottom) show relevant sampling sites from the *Falkor* (Perth Canyon), GEOSECS, WOCE, and CLIVAR cruises.

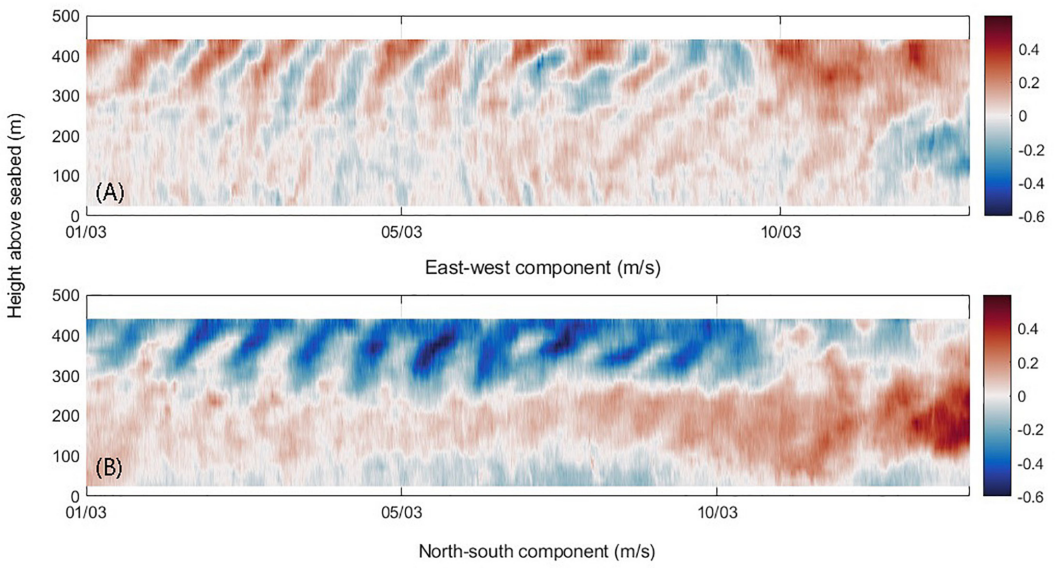

FIGURE 7 | Time series of **(A)** east–west component; and **(B)** north–south component of currents recorded March 1–15, 2015 within the Perth Canyon at 500 m water depth (see location in **Supplementary Figure 9**). Positive values represent currents to the east and to the north.

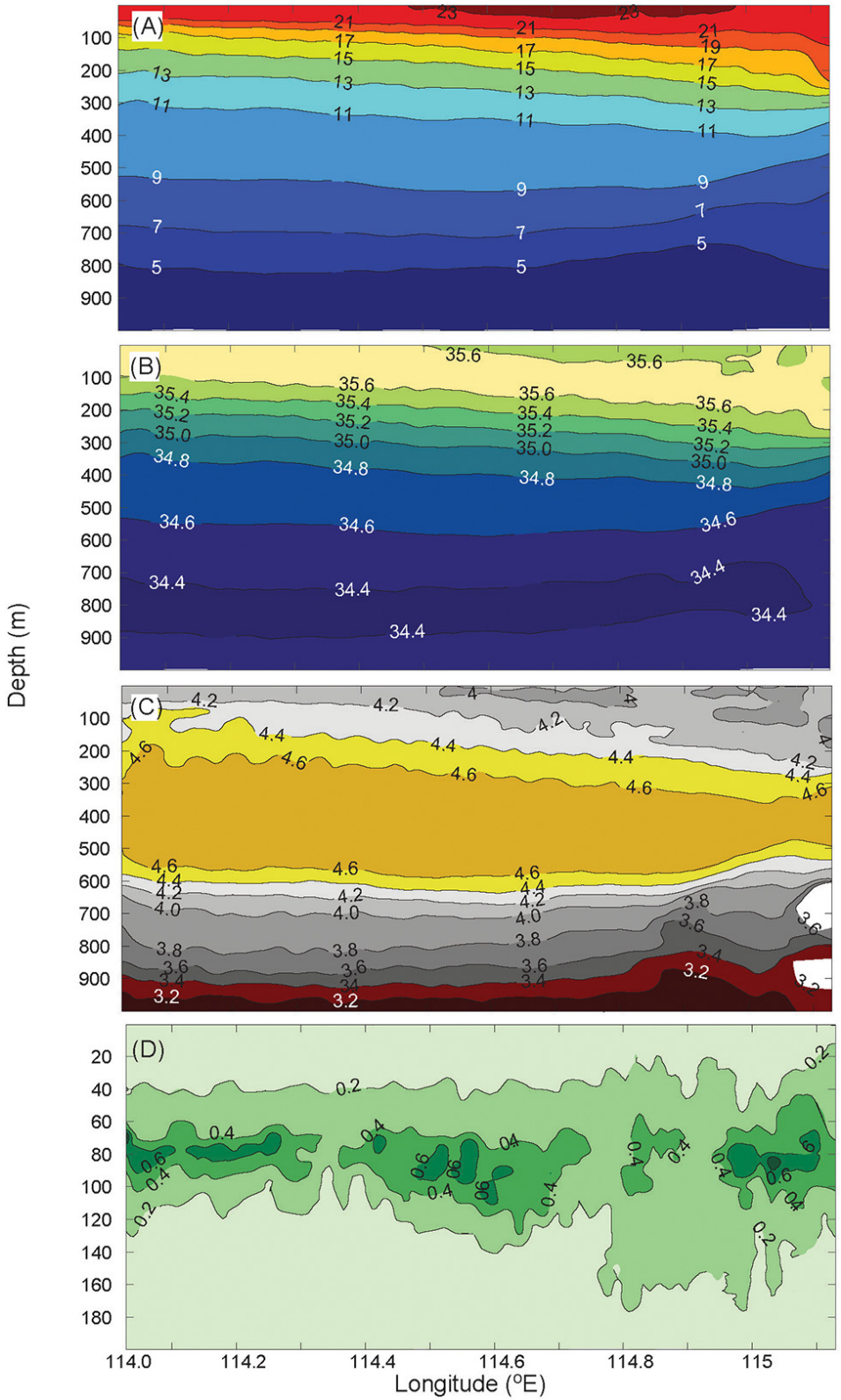

FIGURE 8 | Ocean glider transect across the canyon showing: **(A)** temperature, **(B)** salinity, **(C)** dissolved oxygen, and **(D)** chlorophyll fluorescence. Note that the chlorophyll fluorescence is shown for the upper 200 m.

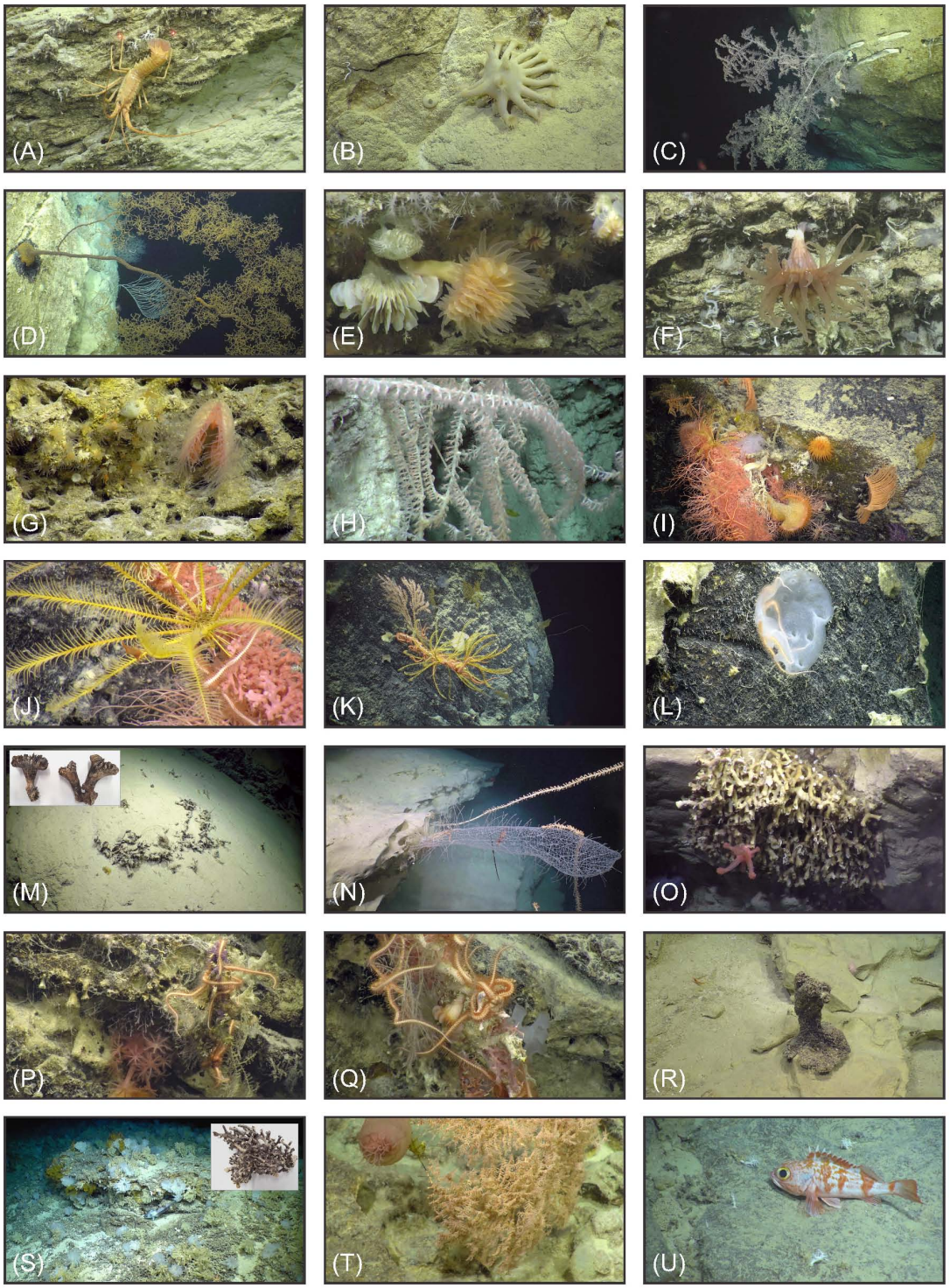

FIGURE 9 | Images of some faunas observed during the ROV dives. Site A: Lobster *Projasus parkeri* **(A)**, hermit crab *Sympagurus* sp. with zoanthid *Epizoanthus* sp. **(B)**, antipatharian corals **(C,D)**, cup corals *Desmophyllum dianthus* **(E)** and *Polymyces* sp. **(F)**, *Acesta* sp. bivalve **(G)**. Site B: bamboo coral **(H)**. Site C: *Corallium* 'community' hosting various taxa **(I)**, crinoid on *Corallium* sp. **(J)**, crinoids and brittle stars on dead bamboo coral **(K)**, hexactinellid sponge **(L)**, fossil coral deposits predominantly *D. dianthus* **(M)**. Site D: *Walteria* sp. glass sponge with comensal shrimp and bamboo coral **(N)**, *Solenosmilia variabilis* colony **(O)**. Site E: brittle stars, *Anthomastus* sp. and dead cup corals **(P)**, *Corallium* sp. with brittle stars and *D. dianthus* **(Q)**, Mn-coated dead *Corallium* stump **(R)**. Site F: hexactinellid sponges, crinoids, and fossil coral deposits predominantly *S. variabilis* **(S)**, pelagic holothurian and antipatharian coral **(T)**, Bigeye Ocean Perch *Helicolenus* sp. and stylasterids **(U)**.

number of bamboo corals (nominally *Keratoisis*), one collected at 933 m (**Figure 9H**) from the weakly lithified beds often observed throughout this shallower part of the canyon system. Gold corals (*Chrysogorgia* and *Iridogorgia)* and purple soft coral seen between 937 and 930 m.

The deepest dive surveyed was at Site C (1,512–1,821 m) within the UCDW, near the junction of the two main canyon tributaries. Depth ranges for different and widely distributed taxa included sea anemones (1,537–1,817 m), live bamboo corals (nominally *Acanella*, *Keratoisis,* and *Lepidisis* at 1,536–1,816 m), live black corals (1,572–1,789 m) and live *D. dianthus* (1,556–1,773 m). Over smaller depth ranges, or in smaller numbers, were *Narella* sp. (1,749–1,766 m), the gold corals *Chrysogorgia* and *Metallogorgia* (1,605–1,796 m; the former collected at 1,793 m), *Anthomastus* spp. (1,567 m), *Paragorgia* (collected at 1,739 m), *Corallium* (1,574–1,690 m), a large purple soft coral (1,561 m), unidentified soft corals (1,548–1,606 m), and gorgonians (1,568–1,577 m). Sea pens (Pennatulacea, at 1,528–1,612 m) were occasionally observed on the soft muddy substrates. Crinoids and brittle stars commonly colonized dead and live octocorals (**Figures 9I,J**), isidids (**Figure 9K**), and hexactinellids (**Figure 9L**). Most notably, a spectacularly diverse community of organisms was hosted by a large *Corallium* frame (collected at 1,557 m), which included Venus flytrap sea anemones (*Actinoscyphia* sp.), a new species of bivalve mollusc (*Acesta* sp. nov.), basket stars (*Euryalina* sp.), crinoids, and a new species of hexactinellid sponge (*Farrea* sp. nov., **Figure 9I**). This sample, like other octocorals that dominated this dive, was attached to hard massive rock that characterized the steep canyon walls at this site. Live scleractinians were rare in these deep waters, however, extensive coral graveyards protruded from the fine sediment aprons (reflecting the quiescent environment) between the canyon walls, at depths of ∼1,560–1,790 m. Potentially thousands of predominantly fossil cup corals, apparently *D. dianthus* (collected at 1,788 m; **Figure 9M** and **Supplementary Figures 1J,L**) together with fossil *S. variabilis* indicate substantial reef development in the past. Scattered on the cliff top were numerous bases of sub-fossil bamboo corals (1,550–1,795 m), much larger than the live specimens observed.

The nearby dive Site D on the opposite (southeast) side of the canyon was surveyed at shallower intermediate depths (834–1,210 m), within AAIW and close to the AAIW–UCDW interface (∼1,000 m). *Walteria* glass sponges (**Figure 9N** and **Supplementary Figure 1C**) were especially numerous along the ridge crest, and one specimen collected at 986 m was hosting a commensal shrimp, *Paralebbeus* sp. nov. Demersal faunas, such as oreodories and grenadiers, were often observed throughout this dive. The occasional sea anemone (maximum depth 1,209 m), black coral (1,186 m), and an unidentified "soft coral" (1,131 m) were also observed. The diversity and abundance of megabenthos increased markedly from ∼1,080 m depth, remaining high to the top of the cliff face at ∼990 m. Within that depth range were numerous live *Anthomastus* spp. (1,004–1,072 m), a stylasterid (1,022 m), gold coral (*Metallogorgia* spp. at 1,077 m), a moderately large number of live bamboo corals (nominally *Keratoisis* and *Lepidisis* at 1,046–1,077 m), and other octocoral species (probably *Corallium* spp. at 988 m). Several large sub-fossil bamboo corals were observed at the base of the cliff. Both live and dead octocoral samples were collected at 1,050 and 1,040 m. Some dead scleractinian cup corals, likely *D. dianthus*, were observed at 1,049–1,178 m, and seemingly long-dead colonies of the colonial *S. variabilis* occurred at 1,040–1,073 m. Part of a recently dead colony of *S. variabilis* was collected at 1,073 m from the canyon wall (**Figure 9O**). Brachiopods were also observed hanging from the walls under small ledges (**Supplementary Figure 2A**).

The westernmost dive, Site E, near the mouth of the canyon has steep topography and was surveyed within the deep UCDW waters (1,241–1,728 m) at similar depths to Site C. Sparse megabenthos at ∼1,600 m were mainly comprised of occasional whip-like black coral. Live cup corals (*D. dianthus* and *Vaughanella* sp.) were sparse (1,357–1,603 m) and occasional dead specimens were attached to the bedrock (**Figure 9P**). A live *Vaughanella* was collected from the canyon wall at 1,472 m (**Supplementary Figure 2L**), and dead *D. dianthus* were collected at 1,498 and 1,444 m. Live bamboo coral (nominally *Keratoisis* and *Lepidisis*) were seen at 1,381 m, one collected at 1,377 m, and scattered individuals were moderately abundant up to the shallowest survey depth of the dive (1,228 m). A *Corallium* collected at 1,357 m (**Figure 9Q**) hosted a small community including colonial and cup corals (*S. variabilis* and *D. dianthus*), a new species of hexactinellid glass sponge (*Farrea* sp. nov.) with its commensal polynoid scale worm, a large ophiuroid (*Ophioplinthaca* sp.), stalked barnacle [*Glyptelasma orientale* (Calman, 1919)], and squat lobster (*Munidopsis* sp.). Here, the canyon wall comprised well-lithified thin interbedded strata with distinctive deformation structures (**Supplementary Figure 2I**). A dead manganese-coated octocoral basal stump (**Figure 9R**) was collected at 1,247 m at the top of the traverse, where the substrate comprised thinly bedded irregularly eroded siltstones.

Above the canyon rim on the northern plateau, Site F represents one of the shallowest dive sites (682–760 m) surveyed within AAIW. Here, extensive coral graveyards (**Figure 9S** and **Supplementary Figures 2N,R**) carpeted the substrate (up to 100% of cover in places), together with large numbers of the hexactinellid sponge, *Aphrocallistes* sp., which comprised the dominant live benthos (**Figure 9S**). These remnants of extensive ancient coral reefs were dominated by the colonial species *S. variabilis* but also contained large numbers of cup corals (*D. dianthus* and *Caryophyllia*). Large scoops of fossil coral rubble and accompanying sponges were collected from 746 to 691 m, the associated hash having contained various taxa including gastropod (e.g., corallivorous epitoniids and *Coralliophila* sp.), bivalves, and thecosomatous pteropod shells. A number of sub-fossil octocoral bases were observed at 692 m (*Keratoisis magnifica,* Dueñas, Alderslade and Sánchez, 2014), 690 m (*Corallium* sp.), one thick and highly eroded sample collected at 683 m, but no bamboo corals were observed. Live cnidarians were sparse, with few representatives of antipatharians (742–745 m, e.g., **Figure 9T**), sea anemones (702–751 m), soft corals, unidentified octocorals (682–747 m), and cup corals (*Polymyces* sp., collected at 739 m), with stylasterids observed throughout the dive. The cup corals were observed close to the substrate, attached to ledges or small overhangs of well-lithified

low-lying beds or fallen blocks. Mobile benthos included various crustaceans, including squat lobsters, hermit crabs (*Sympagurus* sp.) with the commensal zoanthid (*Epizoanthus* sp.), a solitary king crab (*Paralomis dofleini,* Balss, 1911) that is the southernmost record of the species, and few occurrences of echinoderms (sea stars and sea urchins). Large amounts of plankton in the water were observed, such as krill, ctenophores, and salp chains. Pelagic faunas observed included holothurians (**Figure 9T**), various fish (e.g., Bigeye Ocean Perch, *Helicolenus* sp., **Figure 9U**), and a shark.

The most common live scleractinian coral found was the cup coral *Desmophyllum dianthus*, which typically occurred in groups. Other solitary corals observed and collected were *Caryophyllia* sp., *Polymyces* sp., and *Vaughanella* sp. The only colonial scleractinian, *Solenosmilia variabilis*, was found alive as a small colony hosted by *Corallium* (Site E) and as a single polyp on a recently dead colony (Site B). Calcitic octocorals (e.g., *Corallium, Lepidisis*) were also present and collected during most surveys. Live corals were collected from intermediate waters (AAIW) at dive Sites A, B, D, F, and from deep waters (UCDW) at Sites C and E. The main coral taxa found and their associated water masses at each survey depth range are shown in **Figure 10**. Further details of observations and samples collected during the Perth Canyon cruise can be found in the events logs and final cruise report (McCulloch et al., 2017), which can be accessed from the Schmidt Ocean Institute website (see footnote 1). Taxonomic analysis of the collected specimens is ongoing (see section "Future Work").

Ages of Coral Taphocoenoses

U/Th ages determined from the skeletons of dead colonial (*S. variabilis*) and solitary (*D. dianthus*) scleractinians from the two coral graveyard deposits (Sites C and F) are similar, although specimens from the deeper waters span a wider age range (**Figure 11** and **Supplementary Table 4**). Corals collected from deposits of mostly *S. variabilis* (**Figure 9S**), which covered the substrate north of the canyon (Site F) at intermediate water depths (690–720 m), range in age from ∼22 ka to ∼27 ka (BP). The deep water (1,560–1,790 m) deposits with prolific *D. dianthus* (**Figure 9M**) protruding from sediments between the canyon walls in the south of the canyon (Site C), yielded ages from ∼18 ka to ∼33 ka (BP).

DISCUSSION

This study has provided the first video footage and important information about the canyon and its inhabitants, including indicators of anthropogenic effects registered by these waters, which are discussed in detail below. The variably lithified shales/mudstones and sandstones most commonly observed throughout the canyon are similar to reports from earlier studies (Marshall et al., 1989; Shafik, 1991) undertaken on dredge samples recovered from the canyon walls and continental slope during the 1988 *RV Rig* Seismic expedition (BMR Cruise 80). Our Late Paleocene to possibly Early Miocene biostratigraphic ages are also consistent with the main stratigraphic units previously ascribed to the Perth Canyon (**Supplementary Figure 3**), which comprise the Upper Paleocene-Lower Eocene Kings Park Formation, Middle Eocene Porpoise Bay Formation, Upper Eocene Challenger Formation, and the Lower-Middle Miocene Stark Bay Formation (Marshall et al., 1989; Shafik, 1991). We note the discrepancies between our Early Oligocene biostratigraphic ages and late Oligocene-Early Miocene Sr ages for loose samples from the shallower dive sites at the canyon head and plateau (A and F). Here we invoke caution given the potential for dissolution (diagenetic) effects or mixed sampling, however, Miocene foraminifer and nannofossil ages have been reported from prior sampling surveys (Marshall et al., 1989; Shafik, 1991). Notably, the Challenger 1 drill core (WAPET 1975; oil exploration well), collected approximately 50 km south of the Perth Canyon, represents a condensed section (∼240 m thick) of dominantly carbonate lithologies with Late Palaeocene to Late Miocene (Quilty, 1978) planktonic foraminifera, which is equivalent in age to our much thicker Perth Canyon section (∼900 m).

The oceanographic data collected during the cruise are in agreement with all of the previous studies (e.g., Woo and Pattiaratchi, 2008; Rennie S. et al., 2009; Rennie S.J. et al., 2009). Our data re-iterate that, although the LC has a minimal influence on the circulation within the canyon, the LU has a significant influence in water depths of 200–800 m. The LU transports SAMW, containing high DO water that originates from the Southern Ocean, to depths of 200–750 m within the canyon. The CTD on the ROV and ocean glider data sampled to maximum depths of 2,000 m and identified AAIW and UCDW, both containing lower DO concentrations beneath SAMW. Below UCDW (i.e., in depth >2,000 m), previous studies (Woo et al., 2006) have identified Lower Circumpolar Deep Water (LCDW: depth range 2,500–3,500m) and Antarctic Bottom Water (AABW: depth range >3,500 m). The persistent sub-surface chlorophyll maximum present at depths ∼80 m associated with vertical thermal stratification is similar to results reported by Twomey et al. (2007).

Faunal Communities and Habitat Conditions

This expedition located and collected a variety of deep-sea fauna, especially deep-sea corals, and has provided the first 'snap-shots' of this large previously unexplored canyon system, mostly within the depth range where cold water corals normally flourish (∼200–2,000 m). Overall, sessile marine benthos typically inhabited the harder surfaces of the canyon walls, but were sparsely distributed throughout the dives. A variety of organisms were often observed in close spatial association forming diverse communities; for example, various echinoderms, including basket stars were often attached to large coral colonies such as *Corallium* sp., illustrating the tendency of deep-sea marine life to cluster around habitat forming species. Similarly spectacular, was the row of the large glass sponge *Walteria* along the top of the ridge at Site D (also present at Site B) these being the first record of this genus in Australian waters and the Indian Ocean, having previously been reported only from Japan, Kermadec Ridge, and Hawaii. Bivalves (*Acesta*),

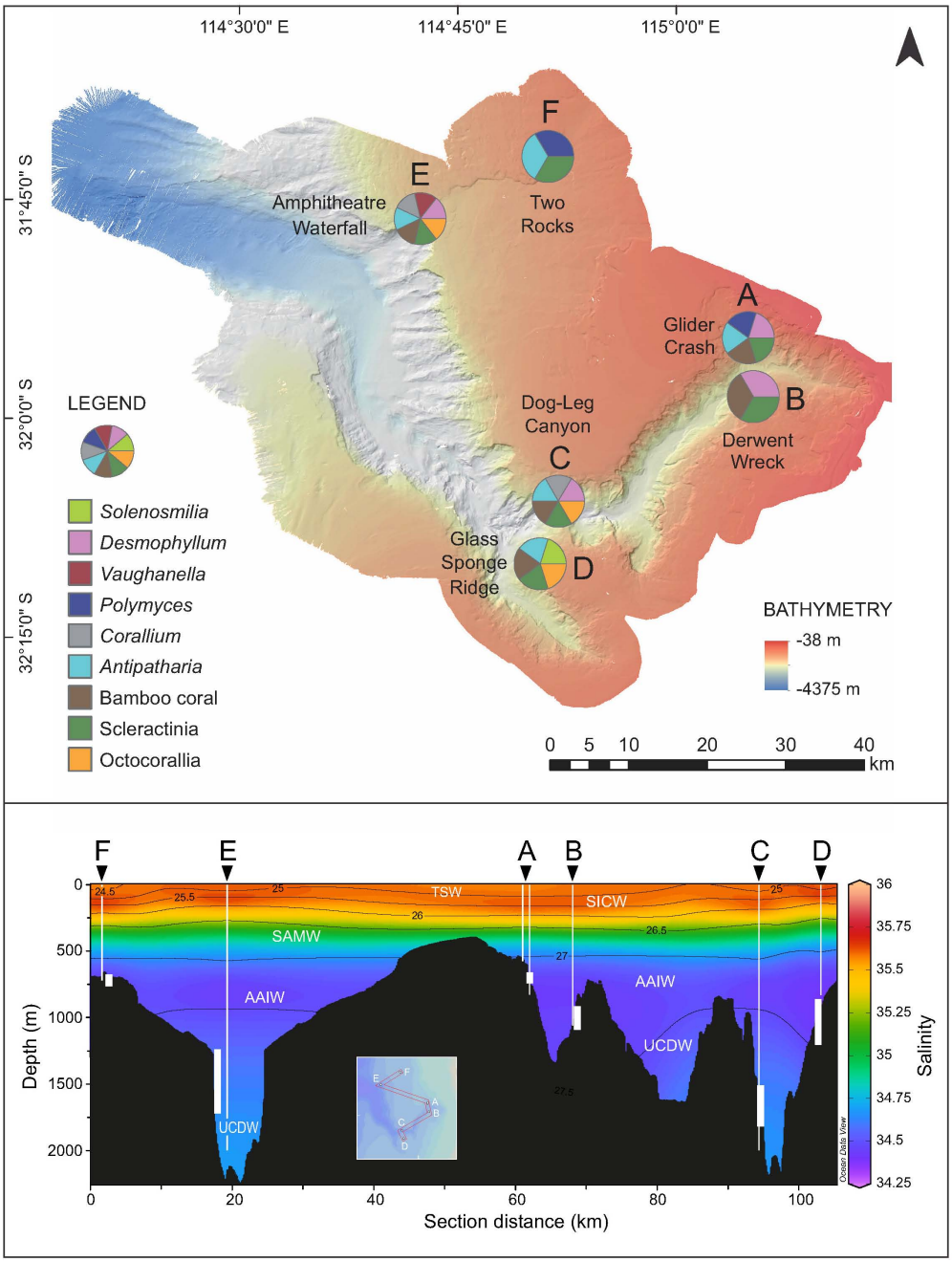

FIGURE 10 | Key coral taxa observed alive during the ROV dives and the relationship of water masses to the dive survey depths. Salinity-depth profile of the canyon waters (bottom) show neutral density contours (kg/m^3), water masses, depth range of each dive (white vertical bars), and CTD casts (white vertical lines). Inset shows path of section to generate seawater profile which is interpolated between sites. TSW, Tropical Surface Water; SICW, Subtropical Indian Central Water; SAMW, Subantarctic Mode Water; AAIW, Antarctic Intermediate Water; UCDW, Upper Circumpolar Deep Water. Sectors of pie charts are not proportional to abundance. Seawater profile generated using Ocean Data View.

occasional brachiopods, and most commonly groups of cup corals (Scleractinia) were found along ledges and overhangs on the canyon walls. Sometimes rows of cup corals, *Desmophyllum dianthus* especially, were found suspended along the moderately lithified and often heavily karstified beds common near the canyon head (**Supplementary Figure 1C**), which provided numerous ledges, crevices, and attachment surfaces. Presumably, this part of the canyon within the upper intermediate waters together with its apparently karstified walls is favorable for these relatively small sessile filter feeders by providing a sufficiently stable substrate, protection from predators, and adequate nutrient supply. However, live specimens of the larger

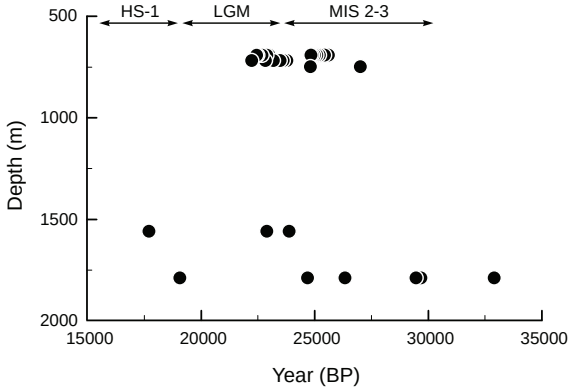

FIGURE 11 | U/Th ages relative to depth distribution of scleractinian corals from the Perth Canyon collected from two dive sites. These fossil coral 'graveyard' deposits occur at Sites C (∼1,500–1,800 m) and F (∼700 m). LGM, Last Glacial Maximum; MIS, Marine Isotope Stage; HS, Heinrich-Stadial.

colonial coral *S. variabilis* are conspicuously rare throughout the dives, which contrasts to their common occurrence in the Tasman seamounts in the South Pacific and Southern Ocean (Thresher et al., 2011). The predominance of this relatively soft and friable lithology, especially in the shallower sites of intermediate water depths, might have played a role in restricting the development of larger mega-benthos, such as colonial coral structures. Gorgonian (*Corallium, Narella*) and bamboo (*Lepidisis*) corals inhabited the greatest depth range through deep and intermediate waters surveyed in the canyon, which is expected given the greater depth of calcite saturation (see below).

The corals were of specific interest, being the target for subsequent geochemical analysis given their importance as environmental archives. They inhabited the cold deep (UCDW) and intermediate (AAIW) waters where temperatures (∼2.5–6°C), pH (7.84–7.98), and DO concentrations (∼150–250 μmol kg^{-1}) are within the ranges commonly reported from other deep sea and/or shallow cold and low pH environments (e.g., fjords) where corals flourish. These water masses are sourced from the Southern Ocean, their compositions including nutrients being almost entirely advected from the south, apart from minimal local contributions via biological export from the surface waters. Furthermore, changes in local hydrography (eddies, upwelling) are essentially limited to shallower depths above the canyon (limited to depths <300 m) and often develop further offshore, thereby affecting the surface water biota as reported elsewhere (Rennie S. et al., 2009; Rennie S.J. et al., 2009). The deeper waters within the canyon appear to be quiescent and lack strong currents (tides have negligible influence), as revealed by expanses of sediment drapes and that ROV deployments did not encounter strong turbulence below the surface currents (>300 m). Thus, the canyon topography has little effect on much of the canyon waters, which is also supported by the consistent seawater characteristics at respective depths across all dive sites.

The absence of sediment input together with the passive deep-water conditions characteristic of the Perth Canyon differ markedly from other canyon systems where rich ecosystems of cold-water corals occur. A dynamic bottom-water regime, such as vigorous bottom currents, internal tides and waves, and downwelling of nutrient-rich surface waters, are critical for enhancing food distribution through the water column, which is important for the development of large coral ecosystems (White et al., 2005; Duineveld et al., 2007; Dullo et al., 2008; Freiwald et al., 2009; Roberts et al., 2009; Rüggeberg et al., 2011; Hebbeln et al., 2014, 2016; Mohn et al., 2014; De Clippele et al., 2018). The relatively sporadic distribution of fauna observed during the Perth Canyon expedition is consistent with a passive canyon scenario, however, we acknowledge that our spatially limited faunal observations might not be representative of the ecosystems potentially inhabiting this large canyon system.

The distribution of calcifiers should also be partly controlled by the carbonate saturation state and pH of the ambient waters. The carbonate chemistry determined from these waters (Sites B, C, and E; **Supplementary Figures 7E,F**) show that the calcite saturation state is above unity ($\Omega_{calcite} > 1$) at all depths sampled (i.e., to 2,000 m), which is consistent with the presence of calcitic corals at the deepest survey depths. Conversely, aragonite saturation reaches unity ($\Omega_{aragonite} \sim 1$) at ∼1,000 m, thus waters below this depth are undersaturated with respect to aragonite yet some aragonitic scleractinian corals (*D. dianthus* and *Vaughanella* sp.) were observed and/or collected from depths of ∼1,360–1,770 m. Similar observations have been made from the Tasman seamounts where corals inhabit waters in which both aragonite and calcite are undersaturated by up to 40% (Thresher et al., 2011). Such observations clearly indicate that scleractinians can calcify their skeletons in undersaturated waters, where the low pH corrosive waters do not appear to have significantly adverse effects on their carbonate skeletons. Existing hypotheses suggest that tissues and organic layers may protect the skeletons from dissolution (Ries et al., 2009; Rodolfo-Metalpa et al., 2011), and prior studies have shown that cold-water scleractinian corals significantly up-regulate their internal pH and saturation state in order to enhance calcification (Anagnostou et al., 2012; McCulloch et al., 2012), which is especially important in these low temperature and low pH environments.

The abundance of coral-bearing taphocoenoses (*D. dianthus* and *S. variabilis*) in the Perth Canyon is also a very significant find. Notably these deposits were discovered at two spatially disparate sites through a large depth range, which clearly indicates that both colonial and solitary cold-water corals flourished during the last ice age. Their ages span the Marine Isotope Stage (MIS) 3–2 transition and the Last Glacial Maximum (LGM) into early Heinrich Stadial 1 (HS-1), with the latter marking the onset of the deglaciation. These ages are equivalent to those of *D. dianthus* recovered from high latitude waters of the Southern Ocean south of Tasmania (Hines et al., 2015) that were collected from depths (∼1,400 to ∼1,800 m) equivalent to the deeper *D. dianthus* deposits (Site C) in the Perth Canyon. The abundance of LGM *S. variabilis* is an interesting contrast to their present-day occurrence, being very rare at the locations we surveyed. These fossil corals will also be important for geochemical studies reconstructing environmental conditions prior to and during the LGM, which is often modeled

to understand ocean-climate dynamics and constraining the carbon budget that underpin predictions of future climate change scenarios.

Anthropogenic Impacts

Despite the proximity of the Perth Canyon waters to a major city and commercial port, the physical imprint of human activities is remarkably absent. The only indicators observed were a stranded oceanographic glider and very minor traces of litter including a fishing net at shallower depths (Sites A and F). Conversely, isotope analyses of seawater samples have shown the ingress of anthropogenic carbon within surface waters, from both nuclear bomb tests and CO_2 emissions, the latter also registered in upper intermediate water depths.

The general profile of $\delta^{13}C$ is similar to those reported previously by Kroopnick (1985) for the eastern Indian Ocean, as well as Sonnerup et al. (2000) and Quay et al. (2003) for the central subtropical (∼20°S) Indian Ocean waters. Those samples were collected further offshore and north of the Perth Canyon during earlier the GEOSECS (1978) and WOCE (1995) cruises. Comparison of prior $\delta^{13}C$ measurements closest to the Perth Canyon, undertaken in 1978 (GEOSECS, station 436), 1995 (WOCE, station 435), and 2009 (US CLIVAR/CO_2, station 189), show continued depletion of ^{13}C within the upper ∼800 m, the 2015 Perth Canyon data having the greatest negative offset of up to ∼0.8‰ (at ∼200 m) from the 1978 profile (**Figure 6**). The highest $\delta^{13}C$ values of ∼1.1‰ of the Perth Canyon waters occur at a depth of ∼500 m, which coincides with the north flowing high oxygen SAMW (**Figure 5**), this being consistent with the global pattern of apparent oxygen utilization as shown by Eide et al. (2017b). This is indicative of the close link between higher O_2 and biologically induced fractionation of $^{13}C/^{12}C$. Furthermore, these results illustrate the complexities of the depth-dependent carbon cycle, with this biologic enrichment in $\delta^{13}C$ being partially nullified by the ingress into surface and upper intermediate water depths of low $\delta^{13}C$ fossil fuel derived carbon (−28‰, Andres et al., 1996). This latter process is commonly referred to as the $\delta^{13}C$ Suess effect, which counters the near surface biologically controlled fractionation of $^{13}C/^{12}C$. Between the years 1978 and 2015, the overall rate of change in seawater $\delta^{13}C$ within the Perth Canyon region that can be ascribed to the $\delta^{13}C$ Suess effect is −0.23‰ per decade. Similar mean decadal declines in ^{13}C have been reported previously for the Indian Ocean and Atlantic subtropics (0.18–0.25‰) with slightly lower means given for the global ocean (Bacastow et al., 1996; Gruber et al., 1999; Sonnerup et al., 1999; Körtzinger et al., 2003; Quay et al., 2003; Eide et al., 2017a).

Seawater radiocarbon ($\Delta^{14}C$) compositions show a similar depth trend to that of existing profiles for the region determined in 1978 (GEOSECS, station 436), 1995 (WOCE station, 435 B), and 2009 (US CLIVAR/CO_2, station 189 B). These profiles systematically diverge within the upper ∼500 m reflecting a decrease of ∼95‰ from 1978 to 2015 in this region. This systematic decrease in upper ocean ^{14}C reflects a combination of processes: (1) the ^{14}C Suess effect, whereby the nuclear bomb ^{14}C produced in the late 1950s and early 1960s is effectively diluted by highly ^{14}C depleted anthropogenic CO_2 released into the atmosphere from fossil fuel burning, reflecting the geologic age ($>10^7$ years) of fossil fuels; (2) the uptake of ^{14}C by both the terrestrial biosphere and upper ocean sinks, the latter process being evident in the depth transects (**Figure 6**); and (3) the decay of ^{14}C ($T_{1/2}$ 5680 years). Recognizing the minor difference in site locations between past oceanographic surveys and this study of Perth Canyon waters, the rate in ^{14}C decline in the upper waters is on average about 28‰ per decade between 1978 and 2015, however, the decadal rate has effectively halved between the two collection intervals, from 40‰ (1978–1995) to 20‰ (1995–2015).

The decline in seawater ^{14}C in this region is approximately 1/3 of the atmospheric rate of decline (∼80‰ per decade) for that period (Orr et al., 2017; Turnbull et al., 2017), consistent with the longer timescales required for isotopic equilibration of the atmosphere and upper ocean, and the ongoing dilution of ^{14}C in the atmosphere by fossil fuel emissions. However, given the competing factor of variable biologically enhanced fractionation of $\delta^{13}C$ as evident in SAMW, reliable deconvolution of the $\delta^{13}C$ Suess effect has significant uncertainties especially in the absence of seasonal profiling. Nevertheless, the penetration depth of ^{14}C (∼500 m) is clearly defined and less than that of ^{13}C (∼800 m), which is consistent with relative penetration depths modeled for mean anthropogenic CO_2, ^{13}C, and ^{14}C and their relative time histories (Quay et al., 2003). Below the upper ∼650 m, the radiocarbon content decreases from −25.6‰ (±2.7, 1σ) to −191.2‰ (±2.6, 1σ) between 651 m and 2,000 m, reflecting the gradual increase in age with depth (from ∼210 to 1,700 years) (**Supplementary Table 3**) and thus the very low ^{14}C content of those older waters.

FUTURE WORK

Taxonomic analysis of the collected specimens is ongoing at the Western Australian Museum, with species descriptions for the hexactinellid sponges (J. Fromont, personal communication), *Acesta* sp. nov. (L. Kirkendale, personal communication), and crinoids (N. Wilson, personal communication) currently in preparation. Further details and analysis of specific faunal habitats will require thorough analysis of all ROV video footage by various specialist taxonomists and ecologists, which is beyond the scope of this study. A large analytical program is currently underway on geochemical proxy studies of both young and fossil corals, a major aim of the cruise being to collect suitable coral species for that work. These archives will provide important environmental records of intermediate to deep waters through major climate events, from the last glacial period as well as modern (pre-industrial to industrial) intervals. Such data are needed to help discriminate long-term natural variations from recent anthropogenic effects that are beginning to impact the deep

ocean. Deep-water corals can therefore play an important role both as archives of environmental change in these poorly studied yet critical areas within the ocean-climate system, and in determining the inherent vulnerabilities and future responses of deep-water ecosystems to global climate change.

CONCLUSION

This study represents our first observations and analysis of samples collected from the Perth Canyon, which have revealed the following:

1. This is a remarkably quiescent 'fossil' canyon system.
2. Fauna are sparse but concentrate in groups forming relatively diverse communities along the canyon walls and rim.
3. Calcifying megabenthos occur throughout the intermediate and deep waters, with some cup corals living below the aragonite saturation horizon ($\sim$ 1000 m).
4. Extensive coral graveyards reveal that deep-water corals thrived in the canyon during the last ice age ($\sim$33 to $\sim$18 ka BP), prior to and during the Last Glacial Maximum.
5. The carbon isotope ($\Delta^{14}C$ and $\delta^{13}C$) compositions of the canyon waters show that anthropogenic carbon has entered upper intermediate water depths between $\sim$600 and 800 m, which has important consequences for the deep-sea calcifiers inhabiting the canyon given the already adverse seawater conditions ($\Omega \sim 1$) under which they must form their carbonate skeletons.

AUTHOR CONTRIBUTIONS

JT, MM, and CP conceived the study. JT, MM, CP, PM, MT, JF, RT, and AH performed fieldwork and data collection. JT, MM, CP, JF, PM, MT, QH, FF, and DH analyzed the samples and/or interpreted the data. JT led the writing of the manuscript. All authors read and approved the final manuscript.

FUNDING

This work was supported by research funding from the Australian Research Council to MM (FL120100049) and JT (FT160100259), the Italian National Programme of Antarctic Research (PNRA16-00069 Graceful Project) to PM and MT, the Australian Institute of Nuclear Science and Engineering to MM, JT, JF, RT, MT, PM (AINSE Award 16/009). Supplementary oceanographic data are funded through Integrated Marine Observing System (IMOS) supported by the Australian Government.

ACKNOWLEDGMENTS

The authors gratefully acknowledge the Schmidt Ocean Institute for providing the RV Falkor and all necessary equipment and crew that enabled us to undertake this cruise (FK150301). The Falkor crew and the ROV pilots from Neptune Marine Services are thanked for their expert assistance during the cruise. Kai Rankenburg (UWA) is thanked for assistance with U/Th mass spectrometry. Ana Hara, Jane Fromont, Oliver Gomez, Lisa Kirkendale, Glenn Moore, and Corey Whisson (from WAM) are thanked for assistance with identifications and specimen processing. The ocean glider and HF Radar data were collected by the IMOS Ocean Glider and ocean Radar facilities located at the University of Western Australia. The mooring data used in this paper were collected by the CSIRO, a sub-facility of the Australian National Mooring Network (ANMN). This is ISMAR-CNR, Bologna scientific contribution n. 1994. Note that some aspects of this paper appear in the pre-print of Trotter et al. (2018) in Biogeosciences Discussions (https://www.biogeosciences-discuss.net/bg-2018-319/).

SUPPLEMENTARY MATERIAL

The Supplementary Material for this article can be found online at: https://www.frontiersin.org/articles/10.3389/fmars.2019.00173/full#supplementary-material

REFERENCES

Anagnostou, E., Huang, K.-F., You, C. F., Sikes, E. L., and Sherrell, R. M. (2012). Evaluation of boron isotope ratio as a pH proxy in the deep sea coral *Desmophyllum dianthus*: evidence of physiological pH adjustment. *Earth Planet. Sci. Lett.* 349, 251–260. doi: 10.1016/j.epsl.2012.07.006

Andres, R. J., Marland, G., Boden, T., and Bischof, S. (1996). "Carbon dioxide emissions from fossil fuel consumption and cement manufacture, 1751 to 1991, and an estimate of their isotopic composition and latitudinal distribution," in *The Carbon Cycle*, ed. T. M. L. Wigely (New York, NY: Cambridge Univ. Press).

Angeletti, L., Taviani, M., Canese, S., Foglini, F., Mastrototaro, F., Argnani, A., et al. (2014). New deep-water cnidarian sites in the southern Adriatic Sea. *Mediterr. Mar. Sci.* 15, 263–273. doi: 10.12681/mms.558

Bacastow, R. B., Keeling, C. D., Lueker, T. J., Wahlen, M., and Mook, W. G. (1996). The 13C Suess effect in the world surface oceans and its implications for oceanic uptake of CO2: analysis of observations at Bermuda. *Glob. Biogeochem. Cycles.* 10, 335–346. doi: 10.1029/96GB00192

Bargain, A., Foglini, F., Pairaud, I., Bonaldo, D., Carniel, S., Angeletti, L., et al. (2018). Predictive habitat modeling in two Mediterranean canyons including hydrodynamic variables. *Prog. Oceanogr.* 169, 151–168. doi: 10.1016/j.pocean.2018.02.015

Brooke, S., and Ross, S. W. (2014). First observations of the cold-water coral *Lophelia pertusa* in mid-Atlantic canyons of the USA. *Deep Sea Res. II* 104, 245–251. doi: 10.1016/j.dsr2.2013.06.011

Canals, M., Puig, P., de Madron, X. D., Heussner, S., Palanques, A., and Fabres, J. (2006). Flushing submarine canyons. *Nature* 444, 354–357. doi: 10.1038/nature05271

Cheng, H., Edwards, R. L., Shen, C.-C., Polyak, V. J., Asmerom, Y., Woodhead, J., et al. (2013). Improvements in 230Th dating, 230Th and 234U half-life values, and U–Th isotopic measurements by multi-collector inductively coupled plasma mass spectrometry. *Earth Planet. Sci. Lett.* 371–372, 82–91. doi: 10.1016/j.epsl.2013.04.006

Company, J. B., Ramirez-Llodra, E., Sardà, F., Aguzzi, J., Puig, P., Canals, M., et al. (2012). "Submarine canyons in the Catalan Sea (NW Mediterranean):

megafaunal biodiversity patterns and anthropogenic threats," in *Mediterranean Submarine Canyons Ecology and Governance*, 1st Edn. ed. M. Würtz (Gland: IUCN), 133–144.

Coplen, T. B. (1996). New guidelines for reporting stable hydrogen, carbon, and oxygen isotope-ratio data. *Geochim. Cosmochim. Acta* 60, 3359–3360. doi: 10.1016/0016-7037(96)00263-3

Cordes, E., Arnaud-Haond, S., Bergstad, O.-A., da Costa Falcão, A. P., Freiwald, A., Roberts, J. M., et al. (2017). "Chapter 42 - cold-water corals," in *The First Global Integrated Marine Assessment: World Ocean Assessment I*, ed. United Nations (New York, NY: Cambridge University Press), 803–816. doi: 10.1017/9781108186148.052

Daly, E., Johnson, M. P., Wilson, A. M., Gerritsen, H. D., Kiriakoulakis, K., Allcock, A. L., et al. (2018). Bottom trawling at Whittard Canyon: evidence forseabed modi?cation, trawl plumes and food source heterogeneity. *Prog. Oceanogr.* 169, 227–240. doi: 10.1016/j.pocean.2017.12.010

Davies, J. S., Howell, K. L., Stewart, H. A., Guinan, J., and Golding, N. (2014). Defining biological assemblages (biotopes) of conservation interest in the submarine canyons of the South West Approaches (offshore United Kingdom) for use in marine habitat mapping. *Deep Sea Res. II* 104, 208–229. doi: 10.1016/j.dsr2.2014.02.001

De Clippele, L. H., Huvenne, V. A. I., Orejas, C., Lundälv, T., Fox, A. Sebastian, H., et al. (2018). The effect of local hydrodynamics on the spatial extent and morphology of cold-water coral habitats at Tisler Reef, Norway. *Coral Reefs* 37, 253–266. doi: 10.1007/s00338-017-1653-y

De Leo, F. C., Smith, C. R., Rowden, A. A., Bowden, D. A., and Clark, M. R. (2010). Submarine canyons: hotspots of benthic biomass and productivity in the deep sea. *Proc. R. Soc. Lond. B.* 277, 2783–2792. doi: 10.1098/rspb.2010.0462

de Vos, A., Pattiaratchi, C. B., and Wijeratne, E. M. S. (2014). Surface circulation and upwelling patterns around Sri Lanka. *Biogeosciences* 11, 5909–5930. doi: 10.5194/bg-11-5909-2014

Douville, E., Sallé, E., Frank, N., Eisele, M., Pons-Branchu, E., and Ayrault, S. (2010). Rapid and accurate U-Th dating of ancient carbonates using inductively coupled plasma-quadrupole mass spectrometry. *Chem. Geol.* 272, 1–11. doi: 10.1016/j.chemgeo.2010.01.007

Duineveld, G. C. A., Lavaleye, M. S. S., Bergman, M. J. N., De Stigter, H., and Mienis, F. (2007). Trophic structure of a cold-water coral mound community (Rockall Bank, NE Atlantic) in relation to the near-bottom particle supply and current regime. *Bull. Mar. Sci.* 81, 449–467.

Dullo, W.-C., Flögel, S., and Rüggeberg, A. (2008). Cold-water coral growth in relation to the hydrography of the Celtic and Nordic European continental margin. *Mar. Ecol. Prog. Ser.* 371, 165–176. doi: 10.3354/meps07623

Eide, M., Olsen, A., Ninnemann, U. S., and Eldevik, T. (2017a). A global estimate of the full oceanic 13C Suess effect since the preindustrial, *Glob. Biogeochem. Cycles* 31, 492–514. doi: 10.1002/2016GB005472

Eide, M., Olsen, A., Ninnemann, U. S., and Johannessen, T. (2017b). A global ocean climatology of preindustrial and modern ocean δ13C. *Glob. Biogeochem. Cycles* 31, 515–534. doi: 10.1002/2016GB005473

Exon, N. F., Hill, P. J., Mitchell, C., and Post, A. (2005). Nature and origin of the submarine Albany canyons off southwest Australia. *Aust. J. Earth Sci.* 52, 101–115. doi: 10.1080/08120090500100036

Fabri, M.-C., Bargain, A., Pairaud, I., Pexdel, L., and Taupier-Letage, I. (2017). Cold-water coral ecosystems in Cassidaigne Canyon: an assessment of their environmental living conditions. *Deep Sea Res. II* 137, 436–453. doi: 10.1016/j.dsr2.2016.06.006

Fabri, M-C., Pedel L, Beuck L., Galgani, F., Hebbeln, D., and Freiwald, A. (2014). Megafauna of vulnerable marine ecosystems in French Mediterranean submarine canyons: spatial distribution and anthropogenic impacts. *Deep Sea Res. II* 104, 184–207. doi: 10.1016/j.dsr2.2013.06.016

Fernandez-Arcaya, U., Ramirez-Llodra, E., Aguzzi, J., Allcock, A. L., Davies, J. S., Dissanayake, A., et al. (2017). Ecological role of submarine canyons and need for canyon conservation: a review. *Front. Mar. Sci.* 4:5. doi: 10.3389/fmars.2017.00005

Fink, D., Hotchkis, M., Hua, Q., Jacobsen, G., Smith, A. M., Zoppi, U., et al. (2004). The ANTARES AMS facility at ANSTO. *Nucl. Instrum. Methods B* 223-224, 109–115. doi: 10.1016/j.nimb.2004.04.025

Freiwald, A, Beuck, L., Rüggeberg, A., Taviani, M., Hebbeln, D., and Meteor Cruise, R. V. M. (2009). The white coral community in the central Mediterranean Sea revealed by ROV surveys. *Oceanography* 22, 58–74. doi: 10.5670/oceanog.2009.06

Gruber, N., Keeling, C. D., Bacastow, R. B., Guenther, P. R., Lueker, T. J., Wahlen, M. H., et al. (1999). Spatiotemporal patterns of carbon-13 in the global surface oceans and the oceanic Suess effect. *Glob. Biogeochem. Cycles* 13, 307–335.

Harris, P. T., and Whiteway, T. (2011). Global distribution of large submarine canyons: geomorphic differences between active and passive continental margins. *Mar. Geol.* 285, 69–86. doi: 10.1016/j.margeo.2011.05.008

Heap, A. D., Edwards, J., Fountain, L., Spinnocia, M., Hughes, M., and Mathews, E., et al. (2008). *Geomorphology, Sedimentology, and Stratigraphy of Submarine Canyons on the SW Australian Slope*. Canberra, ACT: *Geoscience Australia*.

Hebbeln, D., Van Rooij, D., and Wienberg, C. (2016). Good neighbours shaped by vigorous currents: cold-water coral mounds and contourites in the North Atlantic. *Mar. Geol.* 378, 171–185. doi: 10.1016/j.margeo.2016.01.014

Hebbeln, D., Wienberg, C., Wintersteller, P., Freiwald, A., Becker, M., Beuck, L., et al. (2014). Environmental forcing of the Campeche cold-water coral province, southern Gulf of Mexico. *Biogeosciences* 11, 1799–1815. doi: 10.5194/bg-11-1799-2014

Hines, S. K. V., Southon, J. R., and Adkins, J. F. (2015). A high-resolution record of Southern Ocean intermediate water radiocarbon over the past 30,000 years. *Earth Planet. Sci. Lett.* 432, 46–58. doi: 10.1016/j.epsl.2015.09.038

Hua, Q., Jacobsen, G. E., Zoppi, U., Lawson, E. M., Williams, A. A., Smith, A. M., et al. (2001). Progress in radiocarbon target preparation at the ANTARES AMS Centre. *Radiocarbon* 43, 275–282. doi: 10.1017/S003382220003811X

Huang, Z., Nichol, S. L., Harris, P. T., and Caley, M. J. (2014). Classification of submarine canyons of the Australian continental margin. *Mar. Geol.* 357(Suppl. C), 362–383. doi: 10.1016/j.margeo.2014.07.007

Huvenne, V. A. I., and Davies, A. J. (2014). Towards a new and integrated approach to sub-marine canyon research. *Deep Sea Res. II* 104, 1–5. doi: 10.1016/j.dsr2.2013.09.012

Jaffey, A. H., Flynn, K. F., Glendenin, L. E., Bentley, W. C., and Essling, A. M. (1971). Precision measurements of half-lives and specific activities of 235U and 238U, *Phys. Rev. C* 4, 1889–1906, doi: 10.1103/PhysRevC.4.1889

Koenig, S., Fernández, P., Company, J. B., Huertas, D., and Solé, M. (2013). Are deep-sea organisms dwelling within a submarine canyon more at risk from anthropogenic contamination than those from the adjacent open slope? A case study of Blanes canyon (NW Mediterranean). *Prog. Oceanogr.* 118, 249–259. doi: 10.1016/j.pocean.2013.07.016

Körtzinger, A., Quay, P. D., and Sonnerup, R. E. (2003). Relationship between anthropogenic CO2 and the 13C Suess effect in the North Atlantic Ocean. *Glob. Biogeochem. Cycles* 17:10055.

Kroopnick, P. (1985). The distribution of 13C of ΣCO2 in the world oceans, *Deep Sea Res.* 32, 57–84, doi: 10.1016/0198-0149(85)90017-2

Lo Iacono, C., Robert, K., Gonzalez-Villanueva, R., Gori, A., Gili, J-M., and Orejas, C. (2018). Predicting cold-water coral distribution in the Cap de Creus Canyon (NW Mediterranean): implications for marine conservation planning. *Prog. Oceanogr.* 169, 169–180. doi: 10.1016/j.pocean.2018.02.012

Ludwig, K. R., and Titterington, D. M. (1994). Calculation of 230Th/U isochrons, ages, and errors. *Geochim. Cosmochim. Act*a 58, 5031–5042. doi: 10.1016/0016-7037(94)90229-1

Marshall, J. F., Ramsay, D. C., Lavering, I., Swift, M. G., Shafik, S., Graham, T. G., et al. (1989). *Hydrocarbon Prospectivity of the Offshore South Perth Basin*. Canberra, ACT: Bureau of Mineral Resources, Record 1989/23, 158.

McArthur, J. M., Howarth, R. J., and Bailey, T. R. (2001). Strontium isotope stratigraphy: LOWESS Version 3. Best-fit line to the marine Sr-isotope curve for 0 to 509 Ma and accompanying look-up table for deriving numerical age. *J. Geol.* 109, 155–169. doi: 10.1086/319243

McCulloch, M., Trotter, J., Falter, J., Pattiaratchi, C., Montagna, P., Taviani, M., et al. (2017). *ROV Exploration of the Perth Canyon and Assessing the Vulnerability of Deep-sea corals to Climate Change and Ocean Acidification. Schmidt Ocean Institute Cruise FK150301 Final Report*. Available at: https://schmidtocean.org/cruise/perth-canyon-first-deep-exploration/

McCulloch, M., Trotter, J., Montagna, P., Falter, J., Dunbar, R., Freiwald, A., et al. (2012). Boron isotope systematics of cold-water scleractinian corals: internal pH up-regulation and response to ocean acidification. *Geochim. Cosmochim. Acta* 87, 21–34. doi: 10.1016/j.gca.2012.03.027

McLain, C. R., and Barry, J. P. (2010). Habitat heterogeneity, disturbance, and productivity work in concert to regulate biodiversity in deep submarine canyons. *Ecology* 91, 964–976. doi: 10.1890/09-0087.1

Mihanović, H., Pattiaratchi, C., and Verspecht, F. (2016). Diurnal sea breezes force near-inertial waves along Rottnest continental shelf, Southwestern Australia. *J. Phys. Oceanogr.* 46, 3487–3508. doi: 10.1175/JPO-D-16-0022.1

Mohn, C., Rengstorf, A., White, M., Duineveld, G., Mienis, F., Soetaert K. et al. (2014). Linking benthic hydrodynamics and cold-water coral occurrences: a high-resolution model study at three cold-water coral provinces in the NE Atlantic. *Progr. Oceanogr.* 122, 92–104. doi: 10.1016/j.pocean.2013.12.003

Morris, K. J., Tyler, R. A., Masson, D. G., Huvenne, V. I. A., and Rogers, A. (2013). Distribution of cold-water corals in the Whittard Canyon, NE Atlantic Ocean. *Deep Sea Res. II* 92, 136–144. doi: 10.1016/j.dsr2.2013.03.036

Olsson, R. K., Hemleben, C., Berggren, W. A., and Huber, B. T. (1999). Atlas of Paleocene planktonic foraminifera. *Smithsonian Contribut. Paleobiol.* 85, 1–252. doi: 10.5479/si.00810266.85.1

Orejas, C., Gori, A., Lo Iacono, C., Puig, P., Gili, J. M., and Dale, M. R. (2009). Cold-water corals in the Cap de Creus canyon, northwestern Mediterranean spatial distribution, density and anthropogenic impact. *Mar. Ecol. Prog. Ser.* 397, 37–51. doi: 10.3354/meps08314

Orr, J. C, Fabry, V.J., Aumont, O., Bopp, L., Doney, S. C., and Feely, R. A. et al. (2005). Anthropogenic ocean acidification over the twenty-first century and its impact on calcifying organisms. *Nature* 437, 681–686. doi: 10.1038/nature04095

Orr, J. C., Najjar, R. G., Aumont, O., Bopp, L., Bullister, J. L., Danabasoglu, G., et al. (2017). Biogeochemical protocols and diagnostics for the CMIP6 Ocean Model Intercomparison Project (OMIP). *Geosci. Model Dev.* 10, 2169–2199. doi: 10.5194/gmd-10-2169-2017

Pattiaratchi, C., and Woo, M. (2009), The mean state of the Leeuwin Current system between North West Cape and Cape Leeuwin. *J. R. Soc. West. Aust.* 92, 221–241.

Pattiaratchi, C., Woo, L. M., Thomson, P. G., Hong, K. K., and Stanley, D. (2017). Ocean glider observations around Australia. *Oceanography* 30, 90–91. doi: 10.5670/oceanog.2017.226

Paul, D., and Skrzypek, G. (2006). Flushing time and storage effects on the accuracy and precision of carbon and oxygen isotope ratios of sample using the GasBench II technique. *Rapid Commun. Mass Spectrom.* 20, 2033–2040. doi: 10.1002/rcm.2559

Pearson, P. N., Olsson, R. K., Huber, B. T., Hemleben, C., and Berggren, W. A. (eds). (2006). *Atlas of Eocene Planktonic Foraminifera*, Vol. 41. London: Cushman Foundation for Foraminiferal Research, 513.

Playford, P. E., Cockbain, A. E., and Low, G. H. (1976). *Geology of the Perth Basin, Western Australia*. Kalgoorlie: Geological Survey of Western Australia, 124.

Quattrini, A. M., Nizinski, M. S., Chaytor, J. D., Demopoulos, A. W., Roark, E. B., France, S. C., et al. (2015). Exploration of the canyon-incised continental margin of the northeastern United States reveals dynamic habitats and diverse communities. *PLoS One* 10:e0139904. doi: 10.1371/journal.pone.0139904

Quay, P., Sonnerup, R., Westby, T., Stutsman, J., and McNichol, A. (2003). Changes in the 13C/12C of dissolved inorganic carbon in the ocean as a tracer of anthropogenic CO2 uptake. *Glob. Biogeochem. Cycles* 17:1004. doi: 10.1029/2001GB001817

Quilty, P. G. (1978). "The Late Cretaceous-Tertiary section in Challenger No. I (Perth Basin) - details and implications," in *The Crespin Volume: Essays in honour of Irene Crespin*, Vol. 192, eds D. J. Belford and V. Scheibnerova (Basin: Bureau of Mineral Resources), 109–124.

Rennie, S., Hanson, C. E., McCauley, R. D., Pattiaratchi, C., Burton, C., Bannister, J., et al. (2009). Physical properties and processes in the Perth Canyon, Western Australia: links to water column production and seasonal pygmy blue whale abundance. *J. Mar. Syst.* 77, 21–44. doi: 10.1016/j.jmarsys.2008.11.008

Rennie, S. J., Pattiaratchi, C. B., and McCauley, R. D. (2009). Numerical simulation of the circulation within the Perth Submarine Canyon, Western Australia. *Continent. Shelf Res.* 29, 2020–2036. doi: 10.1016/j.csr.2009.04.010

Ries, J., Cohen, A., and McCorkle, D. (2009). Marine calcifiers exhibit mixed responses to CO2-induced ocean acidification. *Geology* 37, 1131–1134. doi: 10.1130/G30210A.1

Roberts, J. M., Wheeler, A., Freiwald, A., and Cairns, S. (2009). *Cold-Water Corals. The Biology and Geology of Deep-Sea Coral Habitats*. Cambridge: Cambridge University Press, 352. doi: 10.1017/CBO9780511581588.003

Roberts, J. M., Wheeler, A. J., and Freiwald, A. (2006). Reefs of the deep: the biology and geology of cold-water coral ecosystems. *Science* 312, 543–547. doi: 10.1126/science.1119861

Rodolfo-Metalpa, R., Houlbrèque, F., Tambutté, E., Boisson, F., Baggini, C., Patti, F. P., et al. (2011). Coral and mollusc resistance to ocean acidification adversely affected by warming. *Nat. Clim. Change* 1, 308–312. doi: 10.1038/nclimate1200

Rüggeberg, A., Flögel, S., Dullo, W.-F., Hissmann, K., and Freiwald, A. (2011). Water mass characteristics and sill dynamics in a subpolar cold-water coral reef setting at Stjernsund, northern Norway. *Mar. Geol.* 282, 5–12. doi: 10.1016/j.margeo.2010.05.009

Sabine, C. L., Feely, R. A., Gruber, N., Key, R. M., Lee, K., Bullister, J. L., et al. (2004). The oceanic sink for anthropogenic CO2. *Science* 305:2. doi: 10.1126/science.1097403

Seddon, G. (2004). *Sense of Place (Facsimile ed.)*. Melbourne: Bloomings Books.

Shafik, S. (1991). Upper cretaceous and tertiary stratigraphy of the Fremantle canyon, South Perth Basin: a nannofossil assessment. *BMR J. Aust. Geol. Geophys.* 12, 65–91.

Skrzypek, G. (2013). Normalization procedures and reference material selection in stable HCNOS isotope analyses – an overview. *Anal. Bioanal. Chem.* 405, 2815–2823. doi: 10.1007/s00216-012-6517-2

Skrzypek, G., and Ford, D. (2014). Stable isotope analyses of saline water samples on a cavity ring-down spectroscopy instrument. *Environ. Sci. Technol.* 48, 2827–2834. doi: 10.1021/es4049412

Sonnerup, R. E., Quay, P. D., and McNichol, A. P. (2000). The Indian Ocean 13C Suess effect. *Glob. Biogeochemi. Cycles* 14, 903–916. doi: 10.1029/1999GB001244

Sonnerup, R. E., Quay, P. D., McNichol, A. P., Bullister, J. L., Westby, T. A., and Anderson, H. L. (1999). Reconstructing the oceanic 13C Suess effect. *Glob. Biogeochem. Cycles* 13, 857–872. doi: 10.1029/1999GB900027

Stuiver, M., and Polach, H. A. (1977). Discussion: reporting of 14C data. *Radiocarbon* 19, 355–363. doi: 10.1017/S0033822200003672

Taviani, M., Angeletti, L., Canese, S., Cannas, R., Cardone, F., Cau, A., et al. (2017). The "Sardinian Cold-Water Coral Province" in the context of the Mediterranean coral ecosystems. *Deep Sea Res. II* 145, 61–78. doi: 10.1016/j.dsr2.2015.12.008

Taviani, M., Angeletti, L., Cardone, F., Montagna, P., and Danovaro, R. (2019). A cold-water coral-bivalve biotope new to the Mediterranean offshore the Naples megalopolis: Just discovered and under threat. *Sci. Rep.* 9:3411. doi: 10.1038/s41598-019-39655-8

Thresher, R. E., Tilbrook, B., Fallon, S., Wilson, N. C., and Adkins, J. (2011). Effects of chronic low carbonate saturation levels on the distribution, growth and skeletal chemistry of deep-sea corals and other seamount megabenthos. *Mar. Ecol. Prog. Ser.* 442, 87–99. doi: 10.3354/meps09400

Trincardi, F., Foglini, F., Verdicchio, G., Asioli, A., Correggiari, A., Minisini, D., et al. (2007). The impact of cascading currents on the Bari Canyon System, SW-Adriatic Margin (Central Mediterranean). *Mar. Geol.* 246, 208–230

Trotter, J. A., Pattiaratchi, C., Montagna, P., Taviani, M., Falter, J., Thresher, R., et al. (2018). Unveiling the Perth Canyon and its deep-water faunas. *Biogeosciences Discuss.* doi: 10.5194/bg-2018-319

Turnbull, J. C., Mikaloff-Fletcher, S. E., Ansell, I., Brailsford, G., Moss, R., Norris, M., et al. (2017). Sixty years of radiocarbon dioxide measurements at Wellington, New Zealand 1954-2014. *Atmos. Chem. Phys.* 17, 14771–14784. doi: 10.5194/acp-17-14771-2017

Twomey, L. J., Waite, A. M., Pez, V., and Pattiaratchi, C. B. (2007). Variability in nitrogen uptake and fixation in the oligotrophic waters off the south west coast of Australia. *Deep Sea Res. II* 54, 925–942. doi: 10.1016/j.dsr2.2006.10.001

van den Beld, I. M. J., Bourillet, J.-F., Arnaud-Haond, S., de Chambure, L., Davies, J. S., Guillaumont, B., et al. (2017). Cold-water coral habitats in submarine canyons of the Bay of Biscay. *Front. Mar. Sci.* 4:118. doi: 10.3389/fmars.2017.00118

van Heuven, S., Pierrot, D., Rae, R., Lewis, E., and Wallace, D. W. R. (2011). *CO2SYS v 1.1, MATLAB Program Developed for CO2 System Calculations. ORNL/CDIAC-105b*. Oak Ridge, TN: Oak Ridge National Laboratory.

von der Borch, C. C. (1968). Southern Australian submarine canyons: their distribution and ages. *Mar. Geol.* 6, 267–279. doi: 10.1016/0025-3227(68)90019-4

Wade, B. S., Olsson, R. K., Pearson, P. N., Huber, B. T., and Berggren, W. A. (eds). (2018). *Atlas of Oligocene planktonic foraminifera*, Vol. 46. London: Cushman Foundation for Foraminiferal Research, 528.

White, M., Mohn, C., de Stigter, H., and Mottram, G. (2005). "Deep-water coral development as a function of hydrodynamics and surface productivity around the submarine banks of the Rockall Trough, NE Atlantic," in *Cold-Water Corals and Ecosystems*, eds A. Freiwald and J. M. Roberts (Berlin: Springer), 503–514.

Wijeratne, E. M. S., Pattiaratchi, C. B., and Proctor, R. (2018). Estimates of surface and subsurface boundary current transport around Australia. *J. Geophys. Res.* 123, 3444–3466. doi: 10.1029/2017JC013221

Woo, M. (2018). *bANFOG Data management User's manual, Version 5.01*. Available at: http://imos.org.au/fileadmin/user_upload/shared/ANFOG/ANFOG_DataManagement_UsersManual_v5.1_21Aug2018.pdf (accessed December 19, 2018).

Woo, M., and Pattiaratchi, C. (2008). Hydrography and water masses off the Western Australian coast. *Deep Sea Res. I Oceanogr. Res. Pap.* 55, 1090–1104. doi: 10.1016/j.dsr.2008.05.005

Woo, M., Pattiaratchi, C., and Schroeder, W. (2006). Dynamics of the Ningaloo current off point cloates, Western Australia. *Mar. Freshw. Res.* 57, 291–301. doi: 10.1071/MF05106

Würtz, M. (2012). "Submarine canyons and their role in the Mediterranean ecosystem," in *Mediterranean Submarine Canyons: Ecology and Governance*, ed. M. Würtz (Gland: IUCN), 11–26.

Yao, W., and Byrne, R. H. (1998). Simplified seawater alkalinity analysis: use of linear array spectrometers. *Deep Sea Res. I Oceanogr. Res. Pap.* 45, 1383–1392. doi: 10.1016/S0967-0637(98)00018-1

Conflict of Interest Statement: The authors declare that the research was conducted in the absence of any commercial or financial relationships that could be construed as a potential conflict of interest.